Geophysical Journal International

Geophys. J. Int. (2012) doi: 10.1111/j.1365-246X.2012.05378.x

Relationships between fault geometry, slip rate variability and earthquake recurrence in extensional settings

Patience A. Cowie,[1]* Gerald P. Roberts,[2] Jonathan M. Bull[3] and Francesco Visini[4]

[1]*School of GeoSciences, University of Edinburgh,* EH8 9XP, *UK. E-mail: patience.cowie@geo.uib.no*
[2]*School of Earth Sciences, Birkbeck College, University of London,* WC1E 7HX, *UK*
[3]*School of Ocean and Earth Science, University of Southampton, National Oceanography Centre, Southampton,* SO14 3ZH, *UK*
[4]*Dipartimento di Scienze della Terra, Università degli Studi "G. d'Annunzio", Campus Universitario di Madonna delle Piane,* 66013 *Chieti Scalo, Italy*

Accepted 2012 January 10. Received 2012 January 10; in original form 2011 March 1

SUMMARY

Field observations and modelling indicate that elastic interaction between active faults can lead to variations in earthquake recurrence intervals measured on timescales of 10^2–10^4 yr. Fault geometry strongly influences the nature of the interaction between adjacent structures as it controls the spatial redistribution of stress when rupture occurs. In this paper, we use a previously published numerical model for elastic interaction between spontaneously growing faults to investigate the relationships between fault geometry, fault slip rate variations and the statistics of earthquake recurrence. These relationships develop and become systematic as a long-term consequence of stress redistribution in individual rupture events even though on short timescales earthquake activity appears to be stochastic. We characterize fault behaviour using the coefficient of variation (CV) of earthquake recurrence intervals and introduce a new measure, slip-rate variability (SRV) that takes into account the size and time ordering of slip events. CV generally increases when the strain is partitioned on more than one fault but the relationship between long-term fault slip rate (SR_{mean}) and CV is poorly defined. In contrast, SRV increases systematically where faulting is more distributed and SR_{mean} is lower. To first order, SRV is inversely proportional to SR_{mean}. We also extract earthquake recurrence statistics and compare these to previously published probability density functions used in earthquake forecasting. The histograms of earthquake recurrence vary systematically as a function of fault geometry and are best characterized by a Weibull distribution with fitting parameters that vary from site to site along the fault array. We explain these phenomena in terms of a time-varying, geometrical control on stress loading of individual faults arising from the history of elastic interactions and compare our results with published data on SRV and earthquake recurrence along normal faults in New Zealand and in the Italian Apennines. Our results suggest that palaeoseismic data should be collected and analysed with structural geometry in mind and that information on SRV, CV and SR_{mean} should be integrated with data from earthquake catalogues when evaluating seismic hazard.

Key words: Palaeoseismology; Continental tectonics: extensional; Dynamics and mechanics of faulting.

1 INTRODUCTION

Slip rate measurements on faults are a fundamental component of our understanding of tectonic activity and earthquake recurrence in a region. Often, however, when we compare slip rate measurements obtained from different sources (e.g. geological, geomorphic and geodetic) over different timescales, there are discrepancies between the rates estimated using different methods (e.g. Oskin *et al*. 2008; Cowgill *et al*. 2009). This is particularly a problem in areas where the regional strain rates are low, earthquake recurrence intervals are long and/or the deformation is distributed across an array of faults (e.g. Faure Walker *et al*. 2010). The lack of consensus between different estimates continues to fuel a debate as to whether geodetically determined rates when compared with longer term geological slip rate estimates reveal true spatial and temporal variations in fault activity (e.g. Dolan *et al*. 2007), or simply highlight observational limitations/bias in the different measurement techniques, for example, short time window of geodetic observations, low age precision

*Now at: Department of Earth Science, University of Bergen, N5020 Bergen, Norway.

© 2012 The Authors
Geophysical Journal International © 2012 RAS

for offset geological and geomorphologic markers and restricted site selection in palaeoseismic trenching. In extensional settings, however, where the constraints are in places relatively good, there is an increasing body of evidence that slip rates vary in space and time and that fault activity is inherently episodic (e.g. Mitchell *et al*. 2001; Benedetti *et al*. 2002; Friedrich *et al*. 2003; Bull *et al*. 2006; Nicol *et al*. 2006; McClymont *et al*. 2009; Schlagenhauf *et al*. 2010, 2011). As the volume of this evidence increases, it becomes important to improve our mechanistic understanding of this behaviour, as well as to characterize variable fault activity, if it is to be of use in informing the collection of new field data and our understanding of seismic hazard. It is this that we aim to do in this contribution.

Existing methods for probabilistic seismic hazard assessment rely heavily on historical seismicity data to derive estimates of earthquake recurrence (the so-called 'Cornell method', Cornell 1971). Increasingly, however, information about the distribution of active faults, long-term fault slip rates and palaeoseismologic data are considered alongside this approach allowing seismic zones to be defined more precisely (e.g. Field *et al*. 2009). For areas of crustal deformation where there are several active faults, and/or the regional strain rate is relatively low the earthquake cycle of some faults is longer than historical records so that the integration of geological and palaeoseismologic data in hazard assessment becomes particularly important (e.g. Pace *et al*. 2006). Key pieces of information that may be derived from palaeoseismic trench studies are (a) estimates of the long-term average earthquake recurrence (T_{mean}) and (b) the variability in recurrence interval on individual faults, which is defined using the coefficient of variation (CV)

$$\mathrm{CV} = \frac{\sigma}{T_{\mathrm{mean}}}, \tag{1}$$

where σ is the standard deviation of the interearthquake times. CV is also referred to as aperiodicity. Several studies acknowledge that CV values for earthquake recurrence intervals are poorly constrained because of limited palaeoseismic records (e.g. Ellsworth *et al*. 1999), yet small differences in CV can lead to order of magnitude differences in probabilistic earthquake forecasts (e.g. Papanikolaou 2003). Moreover, additional assumptions generally need to be made about the underlying probability density function for earthquake recurrence at a particular location otherwise CV simply reflects the dispersion of the data about T_{mean}. Whereas uncertainty and variability in estimates of CV have been widely discussed (e.g. Ellsworth *et al*. 1999; Mucciarelli 2007; Console *et al*. 2008; Parsons 2008), values of long-term average fault slip rate, $\mathrm{SR}_{\mathrm{mean}}$, are assumed to be constant for a particular structure, although the quoted range is often broad because of the combination of limiting factors discussed above.

Modelling has been used to address the issue of why fault slip rates might differ when measured over different timescales. Models show that slip rates vary about $\mathrm{SR}_{\mathrm{mean}}$ if the faults are elastically interacting, that is, transferring stress to adjacent faults when they rupture in an earthquake (e.g. Cowie 1998; Robinson *et al*. 2009). Fault interaction produces temporal clustering of earthquakes, and both the mean earthquake recurrence interval and CV are found to vary between faults within an interacting array (e.g. Robinson *et al*. 2009). However, a limiting feature of many existing models is that constant long-term average slip rates are imposed along pre-defined set of faults (Rundle *et al*. 2006; Robinson *et al*. 2009). Other studies that have investigated the effect of fault interaction on earthquake recurrence (e.g. Zöller & Hainzl 2007; Marzocchi *et al*. 2009), focus on the timescale of seismic catalogues and do not consider patterns of longer term fault behaviour. Some studies have looked at the effects of fault interaction on fault array evolution but mainly from the point of view of the emergence of strain localization, relevant for understanding fault pattern development (Cowie 1998; Narteau 2007). Narteau (2007) discussed how the seismic character of a fault (seismic versus aseismic, etc.) may evolve because of the history of interactions and fault healing but did not deal with the spatial patterns of earthquake recurrence. Lyakhovsky *et al*. (2001) modelled the coupled evolution of earthquakes and strike-slip faults but focused primarily on changes in the size-frequency distribution of the earthquakes. Thus, there are no previous numerical simulation studies that make a link between the spontaneous emergence of a fault network, slip rate variations and earthquake recurrence distributions that develop as faults evolve and interact over the timescale of 100–100 000 yr.

The model from which data herein are analysed is described in more detail by Cowie *et al*. (1993), Sornette *et al*. (1994) and Cowie (1998). Although previously shown to reproduce the power-law scaling of earthquake magnitudes and the fractal structure of fault patterns (Cowie *et al*. 1993, 1995), this is the first time that this model is used to investigate the effect of elastic interaction on fault slip-rate variability (SRV) and earthquake recurrence over tens to hundreds of seismic cycles.

2 DEFINING SLIP RATE VARIABILITY (SRV)

Many studies that discuss variable fault activity (e.g. Friedrich *et al*. 2003) refer to temporal earthquake clustering with intermittent periods of relative quiescence (e.g. Fig. 1; curve (a), produced by the model of Cowie *et al*. 1993). We argue here that such fault activity histories are not adequately described by CV alone as illustrated by the following example. Curve (b) (Fig. 1) shows the exact same temporal order and magnitude of slip events as curve (a) but with the interearthquake times shuffled randomly. For these two curves, CV is by definition identical (= 0.97) because it only depends on the interearthquake times not the order in which the events occur nor the magnitude of slip. Although the average slip rate over 25 kyr is similar (0.2 mm yr^{-1}), there is a variation in slip rate over shorter time periods that is different for the two curves. The highest slip rate, averaged over a time interval of a few thousand years, for curve (a) (Fig. 1) is ≈ 0.85 mm yr^{-1} (at 1.05×10^5 yr), whereas the highest slip rate on curve (b) is ≈ 0.55 mm yr^{-1} (at 1×10^5 yr). This difference arises because of the varying degree of temporal earthquake clustering, that is, the higher slip rate seen for curve (a) coincides with a prominent temporal grouping of larger slip events.

It is clear from the modelled fault rupture histories in Fig. 1 that, to characterize fully the temporal variability in fault activity because of elastic interaction, we require a parameter in addition to CV. Thus we introduce a measure, which we refer to as SRV

$$\mathrm{SRV} = \frac{\sigma_{\mathrm{SR}}}{SR_{\mathrm{mean}}}, \tag{2}$$

where σ_{SR} is the standard deviation of short-term slip rates over a sliding time window of fixed length and $\mathrm{SR}_{\mathrm{mean}}$ is the long-term average slip rate.

Thus if, for example, we fix the time window to 3000 yr for the data shown in Fig. 1, we find that SRV = 1.2 for curve (a), whereas SRV = 0.8 for curve (b) because of the difference in the ordering of the interearthquake times. Basically, the randomization that was applied to curve (b) reduced the preponderance of a clustered sequence of events such as that seen in curve (a). Obviously, alternative random realizations could be presented here but all of

© 2012 The Authors, *GJI*
Geophysical Journal International © 2012 RAS

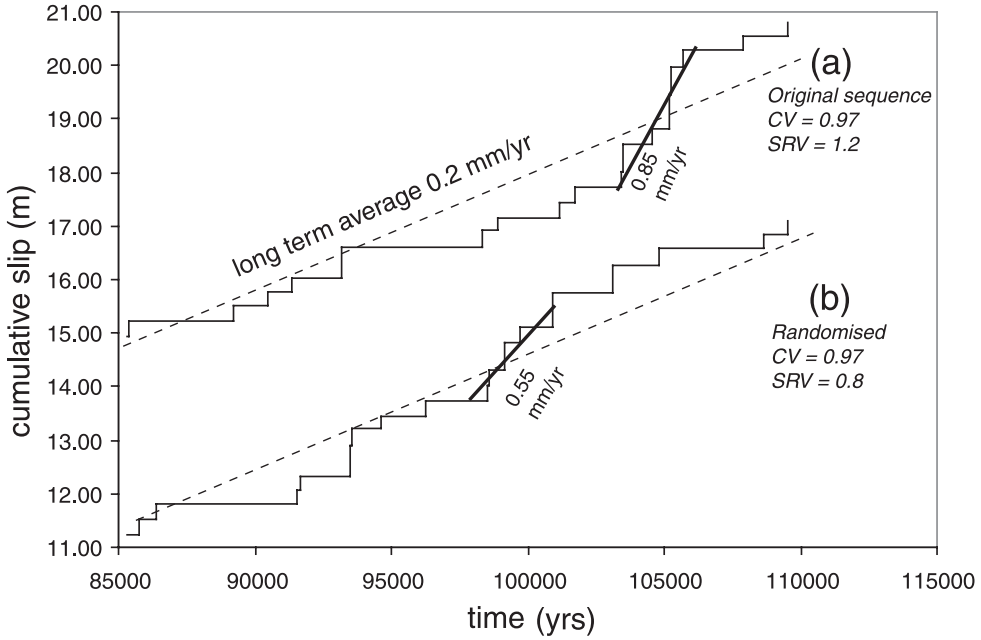

Figure 1. (a) Slip history extracted from numerical model published by Cowie *et al*. (1993). (b) Slip history generated by randomly shuffling the time intervals between successive slip increments in (a). Time window for SRV calculation (eq. 2) is 3000 yr. See Section 2 for explanation.

them would yield the same value for CV whereas SRV would differ for each realisation depending on the reshuffle of interearthquake times as illustrated for one particular example in Fig. 1. SRV therefore provides additional information about the degree of earthquake clustering.

In this study, we use both CV (eq. 1) and SRV (eq. 2) to quantify the pattern of fault slip rate variations and earthquake recurrence over short and long timescales exhibited by the numerical model of fault growth and interaction originally published by Cowie *et al*. (1993). Our aim is to investigate how elastic interaction controls the spatial and temporal variability in fault slip rates and earthquake recurrence. This is a powerful approach because it allows us to derive relationships between fault geometry in map view and fault activity that can be directly compared with a variety of field data from the Whakatane Graben and Taupo Volcanic Zone, New Zealand and the Italian Apennines, where high-quality palaeoseismic and fault slip rate data can be used to validate our conclusions.

3 NUMERICAL MODEL

The model used in this study simulates antiplane shear deformation of a thin elastic-brittle plate using a 2-D square lattice (Cowie *et al*. 1993). The stress perturbation associated with rupture in this model is comparable to that for a Mode III crack with zones of stress enhancement along strike and stress shadows zones located across-strike (e.g. Pollard & Segall 1987). Thus, it is most closely analogous to the development of steeply dipping extensional fault systems. The lattice is made up of 180 × 180 elements that are oriented at 45° to the plate edges. Cyclic boundary conditions are applied in the x-direction to minimize lateral edge effects. A constant velocity is applied along one edge of the lattice ($y = 180$), although the other edge ($y = 0$) is kept fixed. This imposes a uniform antiplane shear strain across the lattice in the direction parallel to the y-axis. Each element is assigned a strength threshold s_c which is drawn randomly from a probability distribution chosen here to be uniform in the interval $(1 - \Delta/2, 1 + \Delta/2)$. These threshold values remain fixed throughout a particular simulation. The elastic shear modulus for all the elements is a constant value. When an element ruptures, it undergoes an instantaneous stress drop by an amount given by $s_c\ \delta/2$ $(0 \leq \delta \leq 2)$. Thus $\delta = 2$ is the case where stress drop is 100 per cent. The magnitude of the offset, or slip, in each rupture is equal to the elastic strain released when the stress drops. For model results presented in Fig. 2 we use $\Delta = 1$ and $\delta = 0.5$, but vary the seed that is used for generating the random distribution of threshold strengths. We also investigate the effect of varying the stress drop parameter δ (Section 4.1).

For a crustal scale model, which we assume here, the size of one lattice element is on the order of 1 km and thus the dimensions of the lattice are ≈130 km and cumulative fault offset is in metres (see Cowie *et al.* 1993, for details). In the simulations shown below the applied plate boundary velocity is 0.001 m yr^{-1} which imposes a constant strain rate across the lattice of 7.7×10^{-9} yr^{-1}. One time step in the model equals about 1 yr. Increments of stress are applied to the whole lattice at each model time step to satisfy the constant velocity boundary condition. When the strength threshold of an element is exceeded, a rupture occurs and the rupture of one element can trigger further breaks. If more than one element fulfils this criterion, the element for which the stress/strength ratio is the greatest is the one that is selected to rupture, followed by rupture of other elements that fulfil this criterion.

An earthquake is defined here as a sequence of ruptures that occur between increments of the plate boundary displacement. Some earthquakes in this model may consist of a single rupture, although others involve a cascade of ruptures of many elements. All the earthquakes are by definition 'large' earthquakes as this is thin plate model so the entire thickness of the plate ruptures. The timing of an individual earthquake is given as an age in years and is determined by the 'model time step' (1 yr) used to apply the loading along the plate boundary. We also use the term 'coseismic time step' to refer to the sequential order of ruptures that occur during one earthquake although it does not have a physical timescale associated with it

© 2012 The Authors, *GJI*
Geophysical Journal International © 2012 RAS

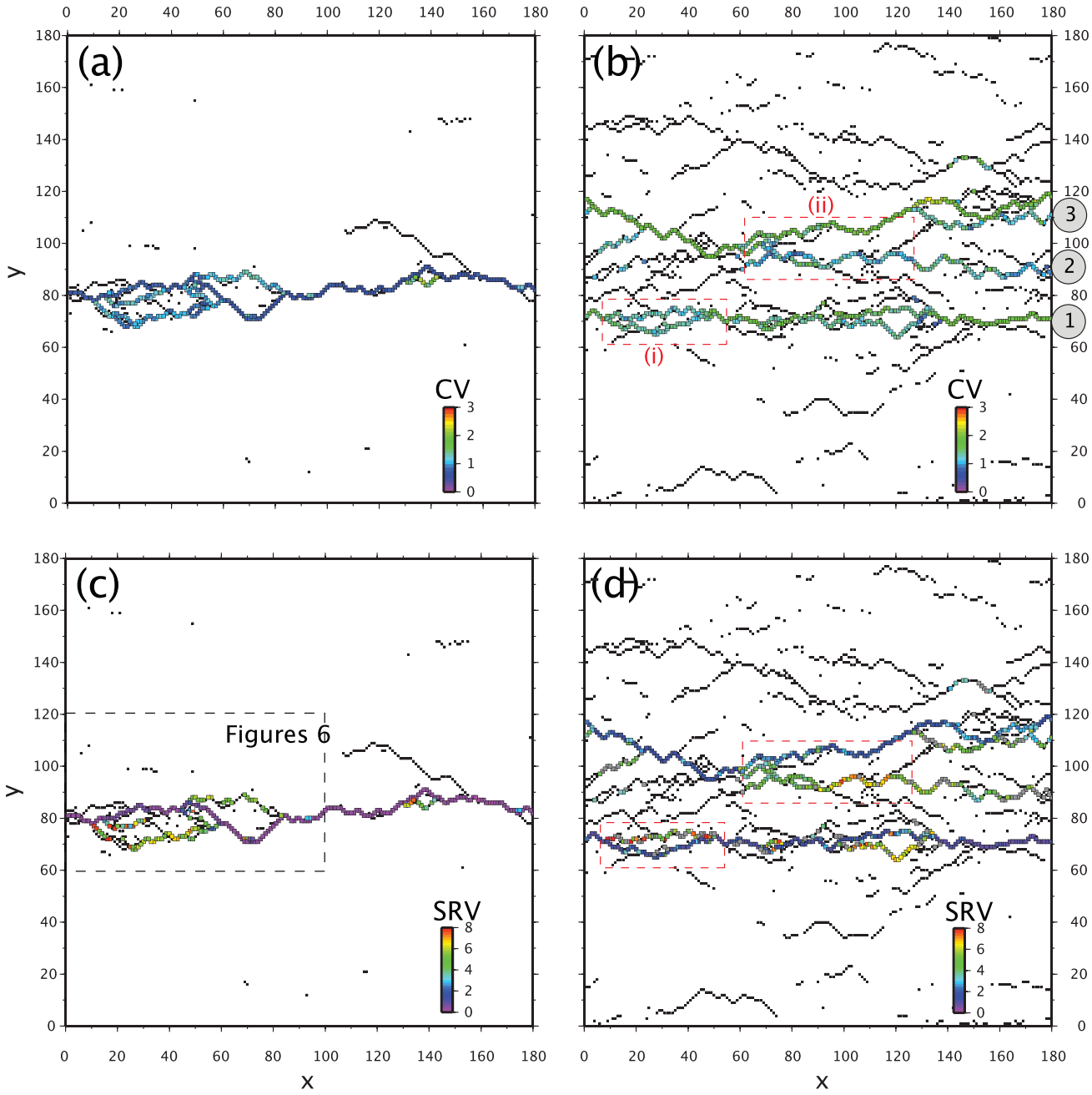

Figure 2. Results of two numerical simulations using different random seeds to produce the spatial variation in strength thresholds but the same δ (stress drop at rupture) and same Δ (range of heterogeneity in strength), see Section 3. Seed 1 (a, c); Seed 2 (b, d). The boundary conditions are identical and the maps represent the fault patterns formed after the same amount of total strain. (a) and (b) show CV variations (in colour) for model elements that ruptured more than 30 times, superimposed on the full fault map (black dots). (c) and (d) show SRV variations (in colour) for model elements that ruptured more than 30 times, superimposed on the full fault map (black dots). Numbers in grey circles (1, 2, 3 in b) refer to the main fault zones plotted in inset to Fig. 3. Red boxes highlight areas discussed in Section 4.1. Black box in (c) shows location of Fig. 6.

in the model. The stress field throughout the lattice is recalculated after each rupture occurs such that the equation of static equilibrium is satisfied at each lattice node (see Cowie *et al.* 1993 for details). Ruptured elements are healed instantaneously and support stress perturbations because of subsequent ruptures even during a cascade consisting of many ruptures. This is analogous to a migrating 'slip pulse' model for earthquakes (e.g. Bouchon 1997) as there is not a synchronous and uniform stress drop along adjacent ruptured elements as a 'crack model' for earthquakes would predict (e.g. King *et al*. 1994).

4 MODEL RESULTS

It has been shown previously that, depending on the seed that is used to create the random spatial variation in threshold strengths, different fault patterns emerge spontaneously from an initially random distribution of ruptures (Cowie *et al*. 1993, 1995). In some cases the deformation is localized onto one major structure (e.g. Figs 2a and c), although in other cases several subparallel faults develop (e.g. Figs 2b and d) and the rupture activity spontaneously migrates across-strike from one fault to another over timescales much longer

© 2012 The Authors, *GJI*
Geophysical Journal International © 2012 RAS

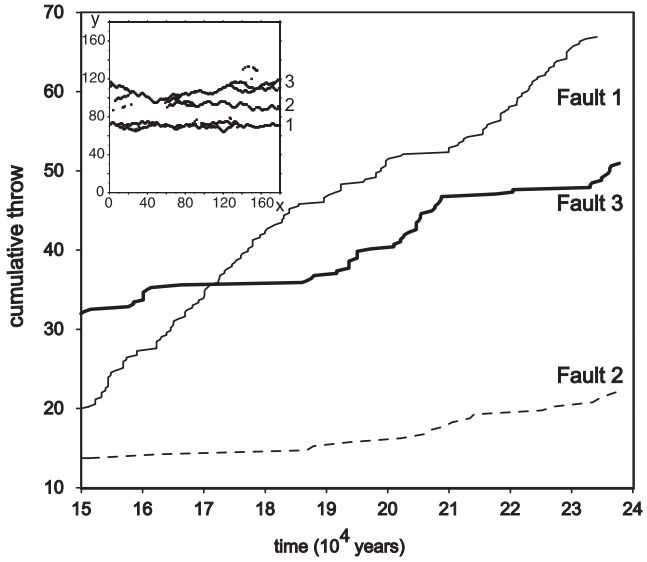

Figure 3. Cumulative fault slip versus time for the fault pattern shown in Figs 2(b) and (d) (see also inset map). Fault 1 develops later than the other faults in this simulation but thereafter is the most localized, highest slip rate fault overall and also shows more persistent activity. There are intervals of time (e.g. 18.5 × 10^4 to 19.5 × 10^4 yr) when all three faults are active, although there are other time intervals (e.g. 17.5 × 10^4 to 18.0 × 10^4 yr) when only Fault 1 is active, or only Faults 2 and 3 are active (e.g. 20.5 × 10^4 to 21.0 × 10^4 yr). Numbers (1, 2, 3) indicate the major faults referred to in Fig. 2(b).

than the typical earthquake recurrence interval (Fig. 3). Natural extensional fault systems commonly show a similar pattern of activity migrating back and forth between subparallel faults, which form a coherent array that over time accommodates a uniform regional extension rate, for example, Nicol *et al*. (2006, 2010).

The areas adjacent to the main faults shown in Fig. 2 show little or no deformation because they lie in the stress shadow of the major zones of strain localization; ruptures occur in these areas during the initial stages of each simulation but become inactive as the deformation localizes. In this study, we focus on the long-term rupture activity of the localized zones (the characteristics of the initial phase of the deformation were discussed by Cowie 1998). Note that all of the features of the numerical model, described below, relating to slip rates and earthquake recurrence arise spontaneously as a consequence of stress redistribution when lattice elements rupture. The only deformation rate that is specified is a constant plate boundary velocity, in contrast to Robinson *et al*. (2009) where slip rates on specific faults are imposed. The main parameter that we consider here is the seed used to generate the random distribution of failure strengths [the range of strength variation, Δ (see Section 3), is kept constant in all the results shown here]. A range of values of the parameter, δ, which governs the stress drop on failure, is also considered to assess how it influences fault slip rate variations.

4.1 Relationships between long-term slip rate, CV and SRV

The two fault patterns shown in Fig. 2 emerge when using two different seeds to generate the spatially random distribution of strength thresholds: Seed 1 (Figs 2a and c) and Seed 2 (Figs 2b and d). The two patterns are plotted after the same total amount of strain. The lattice elements which rupture >30 times are colour-coded to show CV (Figs 2a and b) and SRV (Figs 2c and d). As explained in eq. (2), we obtain SRV by calculating slip rate over a sliding time window of fixed length (in this case 3000 yr), using the value in each time window to obtain the standard deviation in short-term slip rate, σ_{SR}, and then dividing by SR_{mean}, the long-term slip rate averaged over 10^5 yr. The choice of window length for calculating SRV is important in this analysis (Fig. 4). A time window of 3000 yr that we use here is approximately six times the mean recurrence interval ($T_{mean} \approx 500$ yr) along the highest slip-rate portions of the fault network (Fig. 5a). As shown in Fig. 4, for window lengths $\geq$3000 yr and <6000 yr, SRV varies systematically with SR_{mean} but fortunately is relatively insensitive to window length, apart from the portions of the fault network with the lowest $SR_{mean} \leq 0.2$ mm yr^{-1} and/or window length $\leq T_{mean}$ (Figs 4 and 5). Note that SRV gradually decreases as window length increases and in the limit that the window length equals 10^5 yr, σ_{SR}, is by definition zero because the short- and long-term slip rates are the same. For the model data that we present, we find that when the window length is $>\approx$40 kyr SRV ≤ 0.1 for all values of SR_{mean}, consistent with observations from natural fault arrays (Mouslopoulou *et al*. 2009).

For each coloured lattice element shown in Fig. 2, we extracted and investigated the relationships between (1) long-term average slip rate, SR_{mean}, (2) mean earthquake recurrence (T_{mean}; Fig. 5a), (3) CV (Fig. 5b) and (4) SRV (Fig. 5c). The top axis in Fig. 5 refers to the fraction of the total strain rate (1 mm yr^{-1}) that is taken up by a particular structure, that is, how localized or distributed the deformation is. These graphs reveal that, in general terms, the parts of the fault array with higher long-term average slip rate are characterized, as expected, by shorter average recurrence intervals and occur where the deformation is more strongly localized. These higher slip rates sections of the fault array are also characterized by systematically lower SRV values (Fig. 5c), but the relationship between CV and SR_{mean} is less consistent as we discuss further below (Fig. 5b).

Both SRV and CV capture the main differences between a strongly localized pattern of faulting (Figs 2a and c), and a fault pattern where several faults accommodate the deformation (Figs 2b and d) with low values of SRV and CV occurring where the deformation is more localized (Figs 2 and 5). Overall higher values of SRV and CV arise in Figs 2(b) and (d) because of the migration of rupture activity through time back and forth between the main fault zones (Fig. 3) which leads to some long time intervals of quiescence. When specific parts of the fault network are compared, however, CV does not show a simple one-to-one correlation with variations in SRV and SR_{mean} (Figs 5b and c). This is particularly the case for fault strands with low SR_{mean} (< 0.2–0.3 mm yr^{-1}). For example, in the red boxed areas in Figs 2(b) and (d), CV and SRV can be compared for two adjacent fault strands. In box (i), the two strands have similar CV values (CV $\approx$ 1.2), although the SRV values for the same fault strands are very different ($\geq$ 4 compared to $\leq$ 2). In box (ii), the strand at $y = 90$–100 has lower CV (CV $\approx$ 1.2) values along most of its length but higher SRV values (SRV $\geq$ 4), compared to the strand at $y \approx 110$ in box (ii) which has a CV > 2 and SRV $\approx$ 2. As explained in Section 1 (Fig. 1), SRV takes into account the temporal sequence and magnitudes of the fault offsets, not just the interevent times and this provides one explanation for the anomalies highlighted in the red boxes in Figs 2(b) and (d), that is there are real differences in the temporal clustering of the rupture events that are not picked up by CV alone. Furthermore, CV depends on the ratio σ/T_{mean} (eq. 1) so the decrease in CV (seen for average slip rates < 0.2 mm yr^{-1}; Fig. 5b) could be because of either a relative decrease in σ or a relative increase in T_{mean}. SRV is

© 2012 The Authors, *GJI*
Geophysical Journal International © 2012 RAS

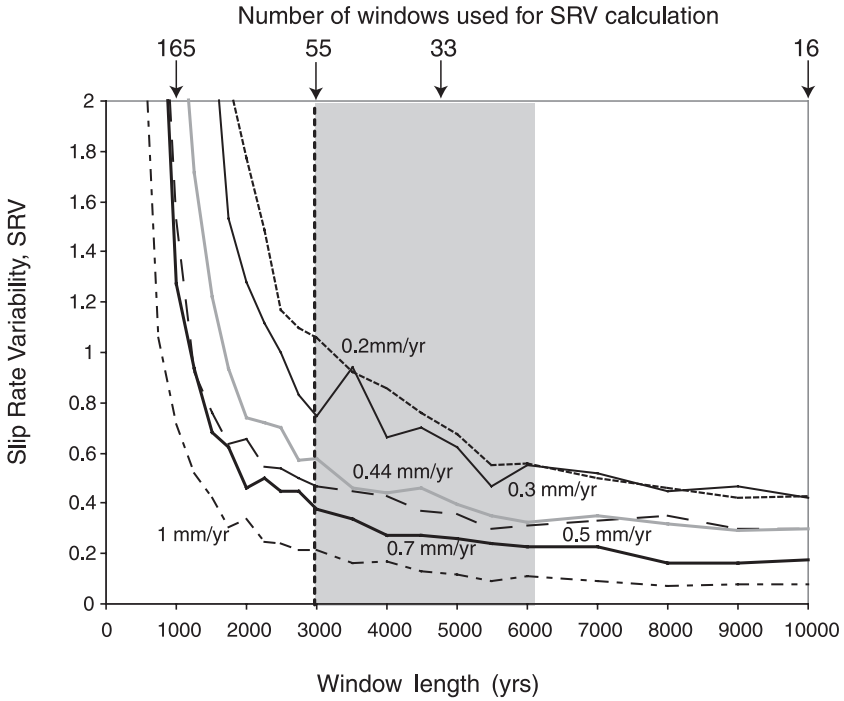

Figure 4. Slip rate variability (SRV, eq. 2) as a function of window length for different values of long-term slip rate, SR_{mean}, using data extracted for different elements in the numerical model (simulation shown in Figs 2a and c). Note that $SR_{mean} = 1\,mm\,yr^{-1}$ means that the element is taking up 100 per cent of the total strain imposed on the plate boundary, that is the deformation has localized onto one row of elements across the model lattice. Dashed line marks window length (3000 yr) used to make maps shown Figs 2(c) and (d). Grey shaded area indicates window lengths for which SRV is sensitive to SR_{mean} but only weakly dependent on window length.

therefore a useful measure that provides new insights that augment what we can learn solely from CV.

Moreover, SRV shows a clear inverse dependence on SR_{mean} that is more consistent than that seen for CV (compare Fig. 5c with Fig. 5b) and furthermore can be quantified. The exact form of the relationship between SRV and SR_{mean} depends on the window length used to calculate SRV but regression of the model data in Fig. 5(c) yields $SRV = SR_{mean}{}^{-1.2}$ with $R^2 = 0.93$. This result is for a window length = 3000 yr, but Fig. 4 confirms that an inverse relationship between these two parameters is robust for a range of window lengths. The segments of the fault network that exhibit highly variable slip histories, with high values of SRV and low SR_{mean} are generally the shorter strands and splays; these connect to through-going faults that are characterized by higher SR_{mean}, low SRV values and thus more uniform slip accumulation through time (when observed over a 3000-yr time window). In contrast to SRV, CV shows large variations (from ≈ 0.7 to > 2) for both fault patterns where $SR_{mean} < 0.2\,mm\,yr^{-1}$ (Fig. 5b). For the fault pattern shown in Fig. 2(a), there is a gradual decrease in CV from ≈ 1.2 to ≈ 0.7 as SR_{mean} increases (red crosses, Fig. 5b) whereas no such relationship is seen for the fault pattern in Fig. 2(b) (blue crosses, Fig. 5b). The lowest values of CV exhibited in the simulations shown here are ≈ 0.7 and occur along the portions of the fault network where SR_{mean} is highest ($\approx 1.0\,mm\,yr^{-1}$) and SRV is low (Figs 5b and c). Note that CV = 0.7 is similar to values used in hazard studies of active extensional faults (e.g. Console *et al*. 2008) and is also similar to the mean value obtained from other modelling studies (e.g. Robinson *et al*. 2009).

The inset graphs, Figs 5(d) and (e), show the dependence of SRV on stress drop, δ. SRV increases approximately linearly with δ (Fig. 5e). The increase is partly because of greater fault offsets when rupture occurs (Fig. 5d) but also because of the fact that the fault pattern becomes less localized and across-strike interaction increases when the stress drop increases. In contrast, CV shows only weak dependence on δ. For the fault array shown in Figs 2(a) and (c) as δ increases from 0.3 to 0.7, the degree of strain localization on the main fault drops from $\approx$100 to 94 per cent, SRV increases systematically from 0.15 to 0.4 but CV only increases marginally from 0.7 to 0.72.

4.2 Site specific fault slip histories

To examine these variations more closely, we have extracted model data for a small area of the model that is shown in Fig. 2(c) and plotted the data in Figs 6 and 7. The map view of the fault pattern is shown in Fig. 6(b) with black lines denoting the broken elements and the colours indicating the antiplane displacement field (which equates to topographic elevation produced by extensional faulting in our analogy). The profiles of total cumulative fault offset (also indicated by the width of the black lines in Fig. 6b) are plotted above for the main fault segments (Fig. 6a). The spatial variations in SRV shown in Fig. 6(c) confirm that the accumulation of slip through time depends strongly on the location of each ruptured element within the fault array. The largest cumulative offsets (Figs 6a and b) develop where the strain is localized onto one major fault with a high long-term average slip rate and low SRV. In contrast, in areas where the deformation is shared between two faults (e.g. $20 < x < 60$) the fault-specific long-term average slip rates are lower and SRV is higher, particularly along the splay fault (Fig. 6c). Fig. 6(d) shows the corresponding spatial variation of CV. Unlike the pattern for SRV, the correspondence between CV and fault geometry is less

© 2012 The Authors, *GJI*
Geophysical Journal International © 2012 RAS

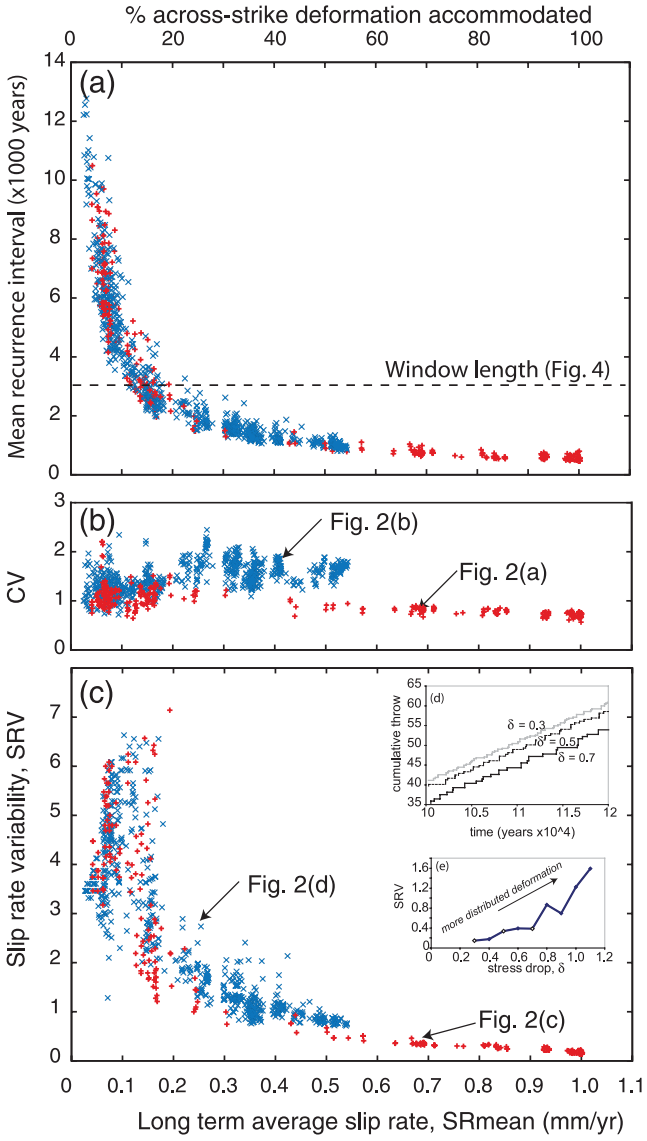

Figure 5. Fault behaviour as a function of long-term average slip rate SR_{mean} using model output plotted in Fig. 2 [red cross (+): Seed 1; blue cross (×): Seed 2]. (a) Mean earthquake recurrence interval, T_{mean} (yr); (b) CV and (c) SRV. Note that top x-axis indicates how localized the deformation is: 100 per cent means that all the deformation is locally taken up by one row of elements across the lattice. T_{mean} and SRV vary systematically with SR_{mean} and a more distributed fault pattern [blue crosses (×)] is characterized by lower SR_{mean}, longer T_{mean} and higher SRV values. CV shows a weak dependence on SR_{mean} most obvious for pattern produced using Seed 1, red crosses (+) (Fig. 2a). Insets (d) and (e) show effect of varying stress drop on fault slip history with $\delta = 0.3, 0.5, 0.7$ illustrated (see Section 4.1 for explanation).

obvious with the exception of the higher CV values along the splay fault. Thus, SRV is capturing temporal earthquake clustering related to fault geometry which is not captured adequately by CV alone.

In Fig. 7, cumulative slip versus time for six different sites within the fault pattern (located in Fig. 6b) are plotted to illustrate the range of fault rupture histories that can arise in the model (see also Table 1). Sites 1 and 2 are located on major fault segments and are characterized by relatively regular slip accumulation through time with no obvious earthquake clustering. At these two sites, $SR_{mean} \approx 1\,mm\,yr^{-1}$, T_{mean} is 500–600 yr, CV $\approx$ 0.7 and SRV $\approx$ 0.2. In contrast, Sites 5 and 6, located on the fault splay, show prominent earthquake clusters with long periods of quiescence with $SR_{mean} \leq 0.2\,mm\,yr^{-1}$, $T_{mean} \approx$ 1550–3200 yr, CV $\approx$ 1.1 and SRV $\geq$ 1.0. The characteristics of cumulative slip at Sites 3 and 4 are intermediate between these two extremes in that the clustering is less marked, the periods of quiescence less prolonged and the long-term average slip rates are roughly half that of the main fault segments. Site 3 is located on a fault segment subparallel to the splay fault and $SR_{mean} \approx 0.5\,mm\,yr^{-1}$, $T_{mean} \approx 800$ yr, CV $\approx$ 0. 9 and SRV $\approx$ 0.5. Site 4 is on a fault segment that is oblique to the main orientation of the fault zone where $SR_{mean} \approx 0.7\,mm\,yr^{-1}$, $T_{mean} \approx 750$ yr, CV $\approx$ 0.8 and SRV $\approx$ 0.4.

The summary statistics shown in Table 1 confirm the spatial variations shown in Fig. 6. As SR_{mean} decreases from 1 to 0.15 mm yr^{-1}, both T_{mean} and SRV increase: SRV increases from 0.2 to $\approx$ 5, and T_{mean} increases from $\approx$ 550 to > 3000 yr. If the lowest slip rate location (Site 6) is ignored because T_{mean} > 3000 yr, which is the window length used to calculate SRV, SRV increases fivefold, from 0.2 to 1.0, as SR_{mean} decreases fivefold (from 1 to 0.2 mm yr^{-1}; see also Fig. 5c). In contrast, CV increases from 0.7 to 1.12 (an increase of only 60 per cent) as SR_{mean} decreases and the relationship is less consistent, especially when the slip rate is low (see also Fig. 5d).

4.3 Earthquake recurrence as a function of fault geometry

The frequency histograms of earthquake recurrence for the same six sites presented in Figs 6 and 7 are plotted in Fig. 8. A key feature of Fig. 8 is that it shows how the histogram shape varies between the six sites consistent with the variations in T_{mean} and CV given in Table 1. The black arrow above each graph shows the recurrence interval that would be expected given the known strength of the element at each site and the far-field loading rate imposed by the plate velocity. For Sites 3 and 4, the position of the arrow approximately coincides with a peak in the histogram but for the other sites it does not. The complex history of stress transfer and triggering between rupturing elements in the model leads to the mismatch between the histogram peak and the position of the arrow in each case (see Section 5.2 for discussion). The prominent peak in some of the histograms (e.g. Sites 1 and 3) might be qualitatively interpreted as indicating a 'seismic cycle' as SRV is relatively low (e.g. Site 1) and the cumulative slip versus time graph appears quasi-periodic (see Fig. 7). It is important to emphasise that the peaked histogram shape emerges spontaneously in this model and are not the result of imposing a rate of moment release on the faults (*cf.* Robinson *et al*. 2009).

All of the histograms show a significant number of short recurrence intervals (≤100 yr), although there is a rapid decline in the number of events when the recurrence interval tends to zero. The shortest recurrence interval observed at all the sites are >0 (on the order of years to decades for the model scaling used here, Section 3). All the histograms are characterized by a long positive tail, comparable to various published probability density functions used to describe earthquake recurrence intervals and to make probabilistic forecasts (e.g. Ellsworth *et al*. 1999).

The Brownian passage time (BPT) model is one of the most commonly assumed probability density functions for earthquake recurrence and it includes both far-field loading of a fault because of plate motions and fluctuations in stress that may be because of coseismic stress transfer, that is, elastic interaction (Matthews *et al*. 2002). As the numerical model we present includes these two effects, it is important to investigate how well the BPT model

© 2012 The Authors, *GJI*
Geophysical Journal International © 2012 RAS

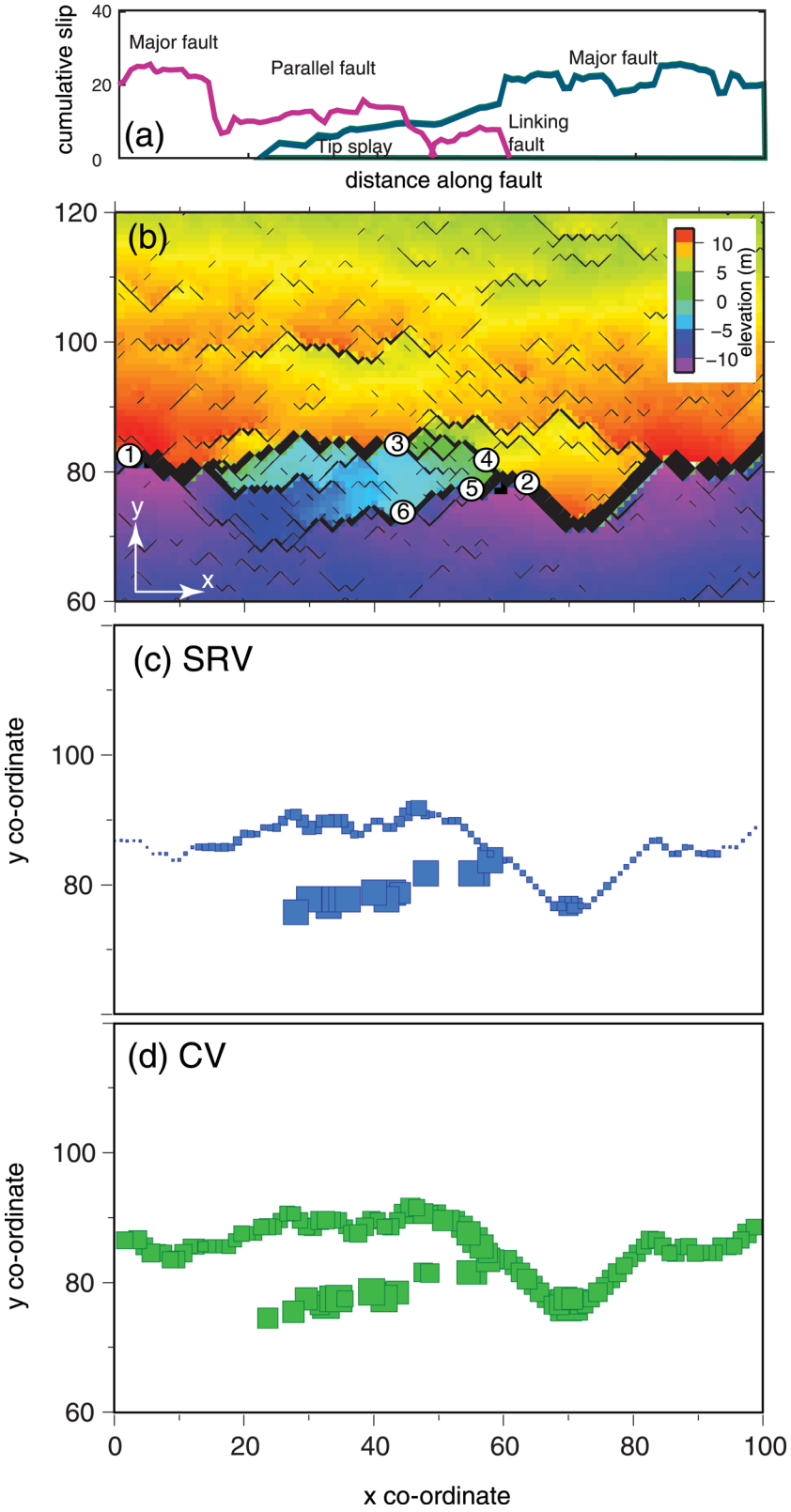

Figure 6. Detailed analysis of variable fault behaviour in a subregion of the model shown in Fig. 2(c) for a 20 000-yr period. (a) Cumulative slip profiles along-strike along the main fault strands marked by heavy black lines in (b). The thickness of the black lines in (b) indicates the total cumulative fault offset, the colours indicate antiplane displacement (= topography in an extensional setting), and numbered sites refer to data plotted in Fig. 7. (c) SRV variations for the main fault strands shown in (b), symbol size proportional to SRV. (d) CV variations for the main fault strands shown in (b), symbol size proportional to CV. Values of SRV and CV calculated for model elements where number of ruptures, $N > 30$.

© 2012 The Authors, *GJI*
Geophysical Journal International © 2012 RAS

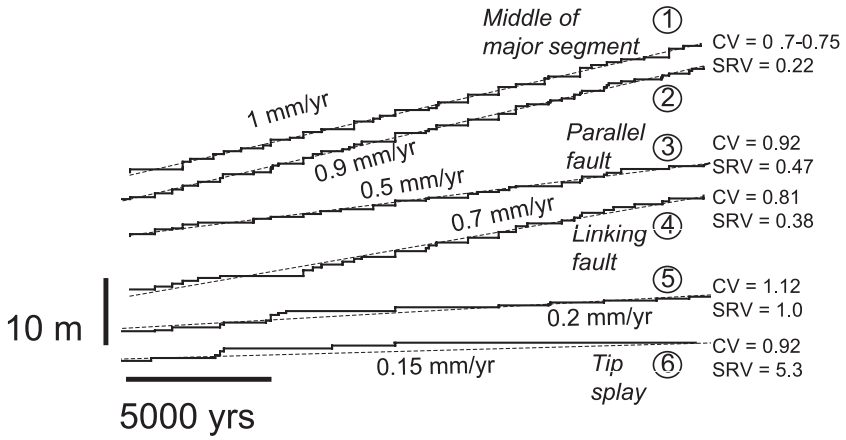

Figure 7. Graphs of cumulative fault slip through time extracted at six points marked along faults in Fig. 6(b) over a time interval of 20 000 yr.

Table 1. Summary of long-term average slip rates, SR_{mean}, earthquake recurrence, SRV and CV for each site shown in Fig. 7 (T_{mean}, mean recurrence interval; T_{median}, median recurrence interval). CV values are calculated using eq. (1). Grey shading indicates sites where an exponential function approximately describes the data (see Table 2).

Site	Strength (0.5–1.5)	SR_{mean} (mm yr^{-1})	Number of earthquakes	T_{mean} (yr)	T_{median}/T_{mean}	CV	SRV (3000 yr)
1	0.783	1	283	583 ±405	0.9	0.7	0.22
2	0.517	0.9	310	532 ±400	0.9	0.75	0.22
3	0.538	0.5	205	806 ±738	0.8	0.92	0.47
4	0.807	0.7	220	747 ±608	0.9	0.81	0.38
5	0.513	0.2	106	1546 ±1732	0.7	1.12	1
6	0.935	0.15	49	3214 ±2947	0.7	0.92	5.3

actually describes our data. The green lines in Fig. 8 are the BPT model constructed using values of T_{mean} and CV derived from the rupture data at each site in eq. (1) (see Table 1). The data sets for all the sites contain large numbers of earthquakes ($\geq$49) so that CV is well constrained for the model data, unlike data sets obtained in the field where more than five earthquakes are rarely recorded and age constraints contribute to uncertainty. We also show for comparison another commonly used distribution, the Weibull distribution. The fitting parameters for the Weibull distribution (β, μ^* and CV*), derived by regression analysis of the recurrence data for each site, are given in Table 2 and are shown by the red lines in Fig. 8. A Weibull distribution has been argued by Zöller & Hainzl (2007) to characterize systems of strongly interacting faults and thus is also relevant to compare with the model output shown here.

The BPT model, constructed with CV values listed in Table 1, provides a reasonable approximation of the recurrence data for some sites (e.g. Sites 1 and 3, Fig. 8). However at very short recurrence intervals (T < 100 yr), the BPT model predicts a smaller number of earthquakes than we observe in the data extracted from the fault model for all the sites considered (green text, Fig. 8). The Weibull distribution (red text, Fig. 8) characterizes the histogram shape for short recurrence intervals significantly better than the BPT model: For Sites 1–5, there is a $\approx$ 30–50 per cent reduction in the rms residuals when the data are fit using a Weibull rather than a BPT model. Note that the Weibull fitting parameters change from site to site; for some sites the Weibull distribution becomes an exponential (Table 2; $\beta \leq 1$, Sites 5 and 6). The values of CV and CV* are comparable (differ by <16 per cent) even though they have been calculated using different methods. The parameter β in a Weibull distribution determines whether the hazard rate increases with time since the last earthquake (β > 1, Sites 1–4), or is approximately constant (Sites 5 and 6), and reflects another important variation in recurrence behaviour between the sites observed in this simulation. To further compare our data with theoretical models we also calculate T_{median}/T_{mean}, which provides an estimate of the skewness of the distributions. For a perfect exponential distribution, this ratio should equal $\log_e(2) = 0.69$. Sites 5 and 6 both have T_{median}/T_{mean} close to this value (Table 1), although the other Sites 1–4 have higher values in the range $\approx$ 0.8–0.9 mirroring the differences in histogram shape.

By subsampling the larger data sets for the other sites (not plotted in Fig. 8), we can confirm that the spatial variation in histogram shape is not a sample size effect but can instead be attributed to a relative increase in the number of recurrence intervals on short timescales (1–100 yr) as well an increase in the number of long recurrence intervals or periods of quiescence, reflected in the variation in values of T_{mean} and CV shown in Table 1. The short timescale effect is because of stress enhancement resulting from along strike ruptures, although the quiescence results from a site being located in a stress shadow, for example, Sites 5 and 6; both effects are the manifestation of elastic interaction seen in the numerical model, as we discuss further below (Section 5.2).

5 DISCUSSION

The results described above demonstrate that systematic spatial and temporal patterns in fault behaviour emerge spontaneously from the combination of uniform regional loading and stress redistribution associated with rupture along the fault zone. In particular, we observe systematic relationships between fault zone geometry, long-term average slip rate, SR_{mean}, variability in slip rate over a short time window (SRV) and to a lesser extent variability in

© 2012 The Authors, *GJI*
Geophysical Journal International © 2012 RAS

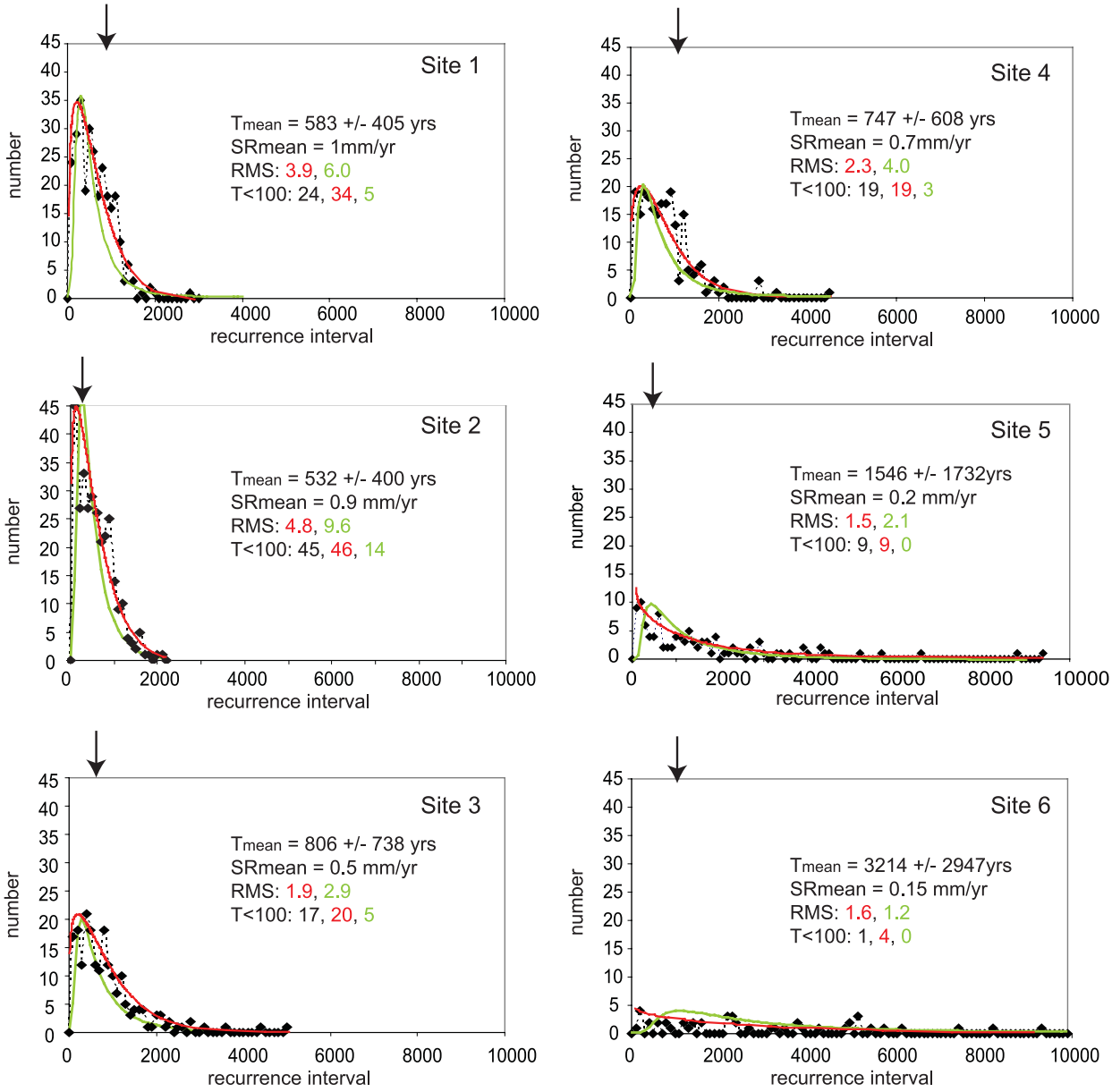

Figure 8. Frequency histograms of earthquake recurrence intervals at the six points shown in Figs 6(b) and 7 over a time interval of 165 000 yr. Bin width is 100 yr. Green line is the BPT model calculated using the T_{mean} and CV for each data set extracted from numerical model (Table 1). Red lines show a best-fitting Weibull model, fitting parameters given in Table 2. $T < 100$ indicates the number of earthquakes which occur in the first histogram bin, black text is the number observed in the numerical model, red and green text refer to the numbers predicted by the Weibull and BPT fits. Note that rms refers to the rms residuals for the Weibull (red) and BPT (green) curves. Black arrow above each graph shows the recurrence interval expected given the known strength of the element at each site and the far-field loading rate imposed by the plate velocity (see Section 4.3 for explanation).

earthquake recurrence, CV (Figs 2–8). Moreover, the histograms of earthquake recurrence extracted at specific locations are comparable to published models of earthquake recurrence probabilities that are thought to provide appropriate descriptions of palaeoseismic data. These are significant results because the variations that we observe emerge spontaneously in our model rather than being defined as initial or boundary conditions.

Our modelling results imply that both SRV and CV should vary spatially in a tectonically active extensional fault array depending on the position and orientation of each fault relative to adjacent active structures. Specifically, lower values of SRV and CV are expected where the deformation is more localized and the long-term fault slip rate is higher (e.g. Figs 5–7). These results are consistent with the modelling study of Robinson *et al*. (2009), which also found an inverse relationship between CV and long-term average slip rate. In this section, we investigate whether these model results are supported by evidence from natural fault systems even though collection of real data on CV and SRV are hindered because of the difficulty of excavating trenches and dating large numbers of palaeoearthquakes in individual trenches.

5.1 Comparison with field data from Italian Apennines and New Zealand

Estimates of CV for real faults are largely derived from palaeoseismological studies of excavated trenches that generally reveal a

© 2012 The Authors, *GJI*
Geophysical Journal International © 2012 RAS

Table 2. Weibull fitting parameters at each site in Table 1 obtained by log-log regression of the cumulative distribution $P(T)$ of recurrence intervals, T, $P(T) = 1 - \exp[-(T/\tau)^{-\beta}]$ (eq. 4 in Abaimov *et al*. 2008). Grey shading indicates sites where the distribution is an exponential, that is, $\beta \leq 1$ (see text for discussion).

Site	τ	β	μ^*	CV*
1	650.9	1.25	605.4	0.81
2	572.8	1.16	544.2	0.87
3	877.2	1.19	824.6	0.85
4	793.9	1.3	730.4	0.79
5	1427.6	0.91	1498.6	1.1
6	3248.7	0.93	3411.2	1.05

μ^*, mean recurrence interval for best-fitting Weibull distribution; CV*, coefficient of variation for best-fitting Weibull distribution.

relatively small number of earthquake ruptures, that is, $\ll$10 events and more typically <5 events. Values of CV quoted in the literature vary from ≈0.1 to ≈1.0 and CV is known to be systematically underestimated when the number of earthquakes is <10 (Ellsworth *et al*. 1999; Console *et al*. 2008; Parsons 2008). Ellsworth *et al*. (1999) and Matthews *et al*. (2002) suggested that a value of CV = 0.5 is a generic estimate for many fault patterns. Our modelling suggests that values of 0.5–0.7 may be underestimates at least in extensional settings where complex fault interactions occur (Table 1).

Statistical tests have been developed to improve the estimates of CV for small samples (e.g. Mucciarelli 2007). However, when coupled with age uncertainties inherent in the sampling constraints and dating methods used, variations in CV related to tectonic setting or tectonic style have been difficult to identify (e.g. Ellsworth *et al*. 1999). Many studies use the approach of assuming an average CV value for a given tectonic province even though fault specific estimates of CV may be available (e.g. Pace *et al*. 2006). This is usually because of the large uncertainty in fault specific estimates of CV (e.g. Peruzza *et al*. 2010). For example, two sites located 14.7 km apart along the Irpinia fault, southern Italian Apennines (Fig. 9), a distance comparable to the length of earthquake ruptures in single large magnitude earthquakes in the region (15–30 km; M_s 6.3–6.9), revealed what may constitute evidence for an along-fault variation in CV as the sites, which are located on different fault segments, do not record exactly the same rupture history. Pantosti *et al*. (1993) interpret the data in terms of the same earthquake sequence and consider the differences as age uncertainties. Using a probabilistic approach to model the combined data, Console *et al*. (2002) obtain one value of CV for the whole fault system, CV = 0.37 ± 0.15, but the quoted uncertainty might reflect a real variation in CV between the two sites (Fig. 9).

Estimates of SRV and CV can also be derived from ^{36}Cl cosmogenic exposure dating of a carbonate fault plane in the Italian Apennines, which has been exhumed by Holocene fault slip (Fig. 9; Schlagenhauf *et al*. 2010). The Magnola fault is a relatively short fault (8 km) compared to other major basin-bounding faults in the region (20–40 km; Roberts & Michetti 2004), which lies within a step-over zone between two major faults (Fiamignano and Fucino faults) with a strike (N105°) that is oblique to the regional fault strike (N145°). It has an average Holocene throw rate of ≈ 0.7 mm yr^{-1} (Papanikolaou *et al*. 2005). Schlagenhauf *et al*. (2010) suggest that five large magnitude earthquakes have exhumed the fault plane by 1.9, 2.3, 0.9, 0.6 and 1.9 m at 7.2, 4.9, 4, 3.4 and 1.5 ka, respectively. They emphasize that this is a minimum number of events, and that each of their modelled slip events could be composed of several smaller slip events closely spaced in time that cannot be resolved. Taking the ages and slip magnitudes for their five events CV = 0.48 and SRV ≈ 0.7 (using window length = 3000). The SRV value is relatively high, but consistent with values for fault splays and faults located in step-over zones that have strikes oblique to the overall fault zone (see Fig. 6 and Table 1). The CV value of 0.48 for this fault is a minimum estimate if small magnitude events, closely spaced in time, have not been resolved (Schlagenhauf *et al*. 2010).

Using palaeoseismological data, Console *et al*. (2008) concluded that, after correcting for sampling bias, most faults in the Italian Apennines should be characterized by CV = 0.7 ± 0.3 (Fig. 9) but two faults in particular are better characterized by lower values of

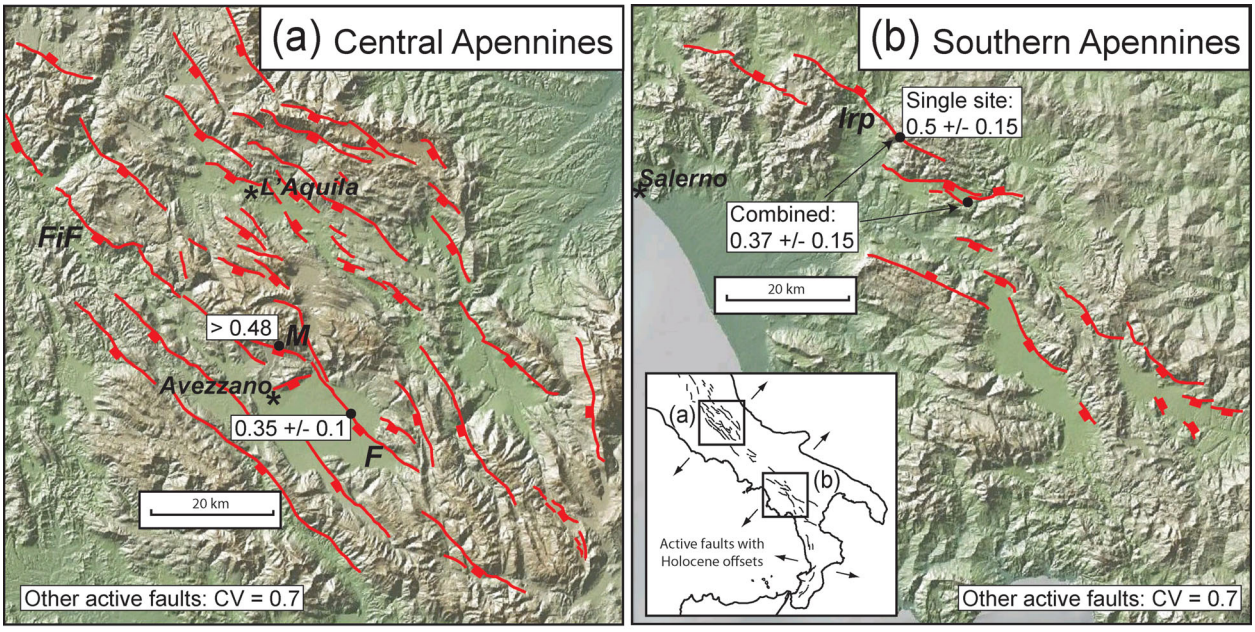

Figure 9. Maps showing locations in (a) the central and (b) the southern Apennines discussed in Section 5.1.

© 2012 The Authors, *GJI*
Geophysical Journal International © 2012 RAS

CV [Fucino = 0.35 ± 0.1 and Irpinia (Colliano) = 0.5 ± 0.15]. Interestingly, the Fucino fault has the highest Holocene slip rate in the central Apennines area of extensional faulting (Pizzi *et al*. 2002; Roberts & Michetti 2004; Papanikloau *et al*. 2005). It is also longer and is less oblique to the regional extension direction than the Magnola fault where CV > 0.48 (see above). These observations are at least consistent with our modelling results, and together this suggests that interaction between faults may provide a physical explanation for the spatial variation in CV inferred by Console *et al*. (2008).

An additional reason why spatial variations in CV are likely to be difficult to identify is that available data on earthquake recurrence may be biased towards faults that have prominent Holocene scarps (e.g. Nicol *et al*. 2009); data from faults with subtle or absent Holocene scarps may receive much less attention unless they rupture. This idea is poignantly illustrated by the occurrence of the M_w 6.3 L'Aquila earthquake in 2009 on the Paganica fault, which had a subdued geomorphic expression compared to the prominent bedrock scarps of neighbouring faults and for which no palaeoseismological data were published before 2009 April (e.g. Falcucci *et al*. 2009; Galli *et al*. 2009; Boncio *et al*. 2010; Emergeo Working Group 2010), despite the existence of palaeoseismic data on neighbouring faults with more prominent geomorphic expressions of Holocene activity. Thus, it may be that the faults most likely to be sampled by palaeoseismologists for recurrence intervals in the field are those with the highest slip rates (whether over just the Holocene or over a longer time period) and the faults that have ruptured in the largest number of events in the Holocene will give the best constrained, and according to our results lower, estimates of CV whereas as lower slip rate structures may be underrepresented. Higher values of CV characterize the parts of the fault zone with low long-term average slip rates and long recurrence intervals that are less likely to be studied (e.g. Figs 6d and 7). Consequently, the true variation in CV across a region containing many faults with varied slip rates and recurrence intervals may be underestimated with the lower estimated values of CV better constrained and thus the most likely to be used in hazard studies.

To calculate robust estimates of SRV, sufficient time resolution is needed to resolve changes in slip rate, but a long enough record is also required to allow the magnitude of slip rate changes to be quantified relative to the long-term average rate. An extensional fault system for which this exceptional quantity and quality of data is available is the Rangitaiki Fault, offshore Whakatane Graben, New Zealand (Fig. 10, Bull *et al*. 2006). Bull *et al*. used high resolution seismic reflection imaging of the uppermost 60 m of a known sedimentary stratigraphic sequence to constrain fault behaviour over the last 17 kyr over 10 different time periods some as short as *ca*. 2 kyr. Displacement profiles for individual segments are increasingly irregular for shorter time periods, and show points of zero rupture where there is structural complexity (see Fig. 11 in Bull *et al*. 2006). The maximum displacement rate over 17 kyr on the Rangitaiki Fault is $3.6 \pm 1.1\,\mathrm{mm\,yr^{-1}}$. We know that these data document 'steady-state' fault behaviour over the last 17 kyr, rather than fault growth phenomena, as Taylor *et al*. (2004) have already showed that the fault grew by segment linkage over *ca*. 1 Ma, and became fully linked between 300 and 17 kyr BP.

We calculated SRV and average slip rate along two of the central segments (R3 and R4) of the Rangitaiki Fault (Fig. 10). SRV (eq. 2) was calculated for the six, five, four and three shortest time periods, with the six shortest corresponding to periods less than or equal to 8.0 kyr; the three shortest to periods less than or equal to 3.1 kyr (see Table 2 in Bull *et al*. 2006). The long-term average slip rate for each segment is calculated by finding the overall mean of the slip rates for the 10 time periods resolved. R3 has the highest average slip rate towards it centre, although slip rate is locally reduced where there is an intersection with an antithetic fault (Point 2, Figs 10a and c), and where the segment splays (Point 3, Figs 10a and c). Conversely, SRV is highest where slip rates are low, and where the deformation is transferred from one fault to an adjacent fault, R4, along strike. Similarly, R4 has slip rates reducing towards the segment tips and at the intersection with the tip of R3 (Point 4, Figs 10b and c). Again, SRV is high at the segment tips where there is overlap between R3 and R4. The changes in SRV along-strike along the fault array may be explained by the variation in the size and position of individual earthquakes. Larger events would rupture the entire fault plane, with smaller events having irregular slip profiles and failing to rupture across segments or asperities along the fault plane. Hence, SRV is greatest at where faults intersect with other structures, or become splayed, and at the tips of segments (Bull *et al*. 2006).

Another field example that supports our modelling results is shown in Fig. 11 where rupture histories are plotted for three active normal faults in the Taupo Volcanic Zone, New Zealand. The regional strain rate in this area is accommodated by an array of subparallel faults (e.g. Fig. 11b), which rupture at different times and exhibit different long-term average slip rates, similar to the behaviour seen in our numerical model (Fig. 3). Nicol *et al*. (2010) already showed for this fault array that the earthquake recurrence interval is more variable, that is, CV is higher, along lower slip rate faults, supporting our model results (Figs 5b and 7). The data plotted in Fig. 11(a) furthermore support our result that SRV varies inversely with $\mathrm{SR_{mean}}$. We have calculated SRV for each of the sites (M1, S1 and T3) by deriving the slip rates between the dated horizons (black dots in Fig. 11a) and using these values to obtain σ_{SR} and $\mathrm{SR_{mean}}$ and hence SRV (eq. 2). The average window length using this approach is 3400 yr but similar values of SRV were obtained when a fixed window of 3000 yr was used. We find that for site M1, where the average slip rate is low, $\mathrm{SR_{mean}} = 0.08 \pm 0.02\,\mathrm{mm\,yr^{-1}}$ (over 25 kyr), $\mathrm{SRV} = 1.6 \pm 0.1$, whereas at site T3 the average slip rate is higher ($\mathrm{SR_{mean}} \approx 0.19 \pm 0.02\,\mathrm{mm\,yr^{-1}}$ over 18 kyr) and SRV is lower (0.8 ± 0.1). At site S1, the average slip rate is intermediate between M1 and T3 ($\mathrm{SR_{mean}} \approx 0.13 \pm 0.02\,\mathrm{mm\,yr^{-1}}$ over 22 kyr) and $\mathrm{SRV} = 0.9 \pm 0.05$, intermediate between the SRV values obtained at the other two sites. Although this is a small sample, these data indicate that $\mathrm{SRV} = \mathrm{SR_{mean}}^{-0.8}$, which is a similar relation to that found for the model data (Fig. 5c). These values of SRV are relatively high values, consistent with the observation that deformation in the Taupo Volcanic Zone is distributed and shared between subparallel faults across the array (Nicol *et al*. 2010) as shown in Figs. 2(b), (d) and 3.

5.2 Structural control of earthquake recurrence histograms

Zöller & Hainzl (2007) previously argued that the Weibull distribution provides a better description of earthquake recurrence intervals if there is strong fault interaction whereas the BPT distribution characterizes isolated or weakly coupled faults. Specifically, they show that strong elastic interaction between faults provides an explanation for the significant number of earthquakes with short recurrence times compared to the BPT model. This is also what we found here (Fig. 8), but in addition we find that the Weibull fitting parameters (Table 2) vary systematically with position along the fault array. This result is entirely consistent with the idea that fault geometry fundamentally controls rupture initiation and propagation and

© 2012 The Authors, *GJI*
Geophysical Journal International © 2012 RAS

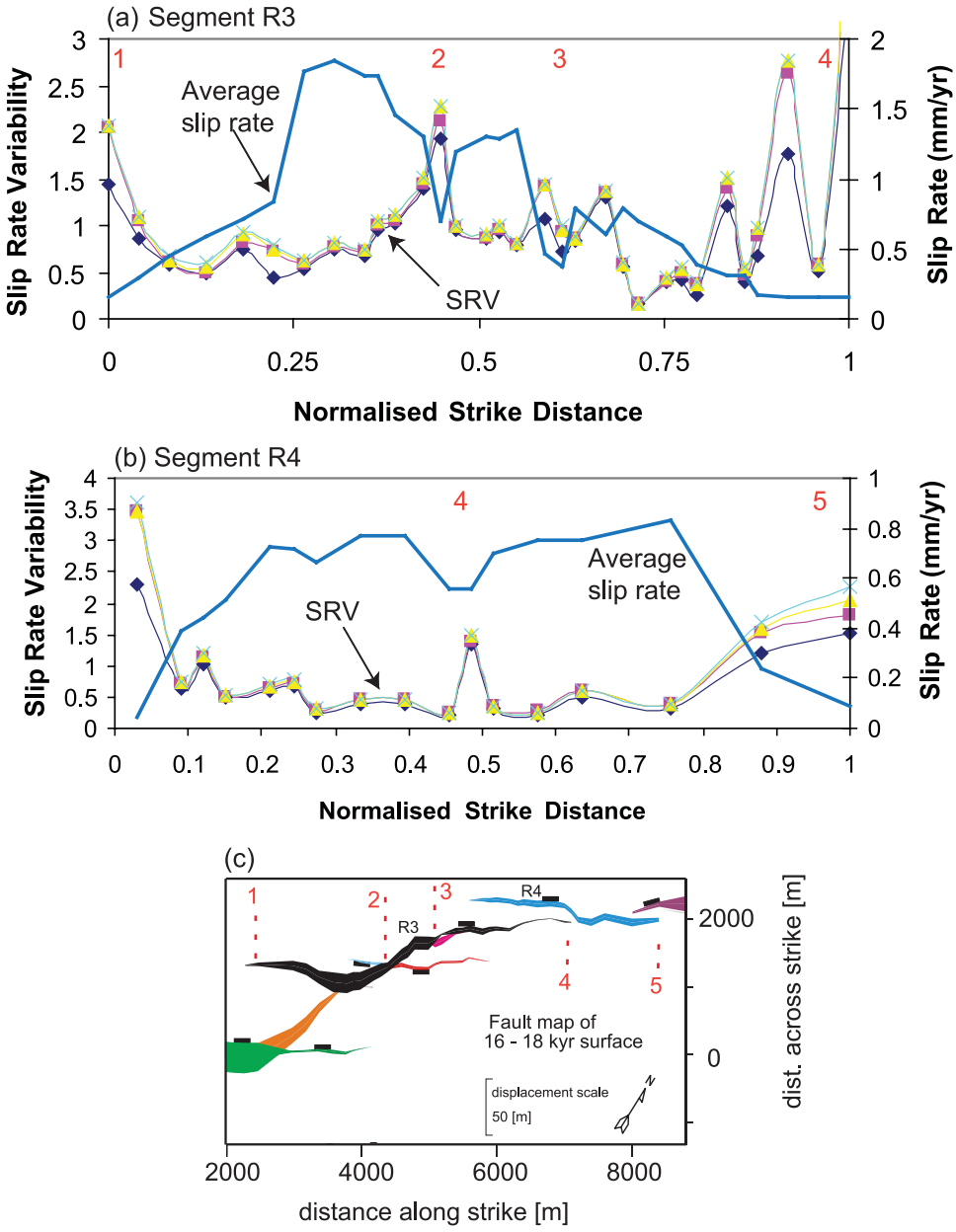

Figure 10. Data on slip rate variability (SRV) for a normal fault array in the Whakatane Graben, New Zealand (reprocessed from data published by Bull *et al*. 2006). Long-term average slip rate along strike (SR_{mean}, dark blue solid line) and SRV (coloured lines) for fault segments R3 and R4. SRV is calculated over different time windows (see Section 5.1 for explanation). (c) Shows map view of fault array with locations of segments R3 and R4 indicated. Red numbers 1–5 in (c) show locations indicated in graphs (a) and (b).

thus presumably also controls elastic interaction both spatially and through time.

To illustrate this idea, we plot in Fig. 12 the variations in stress levels, normalized to strength, for two lattice elements (Sites 4 and 5, Fig. 6b) during two different earthquakes (Earthquake 1 in Fig. 12a and Earthquake 2 in Fig. 12b). The points in time at which rupture occurs are denoted by the stars and coincide with sharp peaks in stress followed by a rapid stress drop. Note that the horizontal axis in Fig. 12, labelled 'coseismic rupture number', refers to the sequential order of ruptures that comprise one earthquake and is distinct from the 'model time step' measured in years (see Section 3). The stress level is recalculated after each rupture as explained in Section 3. Because of the instantaneous healing the stress level in an element can increase rapidly again after a rupture has occurred such that an element may rerupture during the same earthquake (e.g. Fig. 12b).

The stress level on these elements is initially fairly constant and below the threshold for rupture (stress–strength ratio ≈ 0.85–0.95). The stress level starts to change, at first slowly and then more rapidly, because of the increasing proximity of ruptures occurring along-strike along the fault. In some cases, the stress decreases (unloading), although in other cases the stress increases (loading) depending on the rupture trajectory (see inset map). When rupture occurs at Site 4, the stress level at Site 5 decreases significantly, that is, it is unloaded (Fig. 12a). Similarly, when rupture occurs at Site 5, the stress level at Site 4 decreases significantly (Fig. 12b). The unloading effect is produced because these two sites are located in a zone where the fault system splits into two strands so that Site 4

© 2012 The Authors, *GJI*
Geophysical Journal International © 2012 RAS

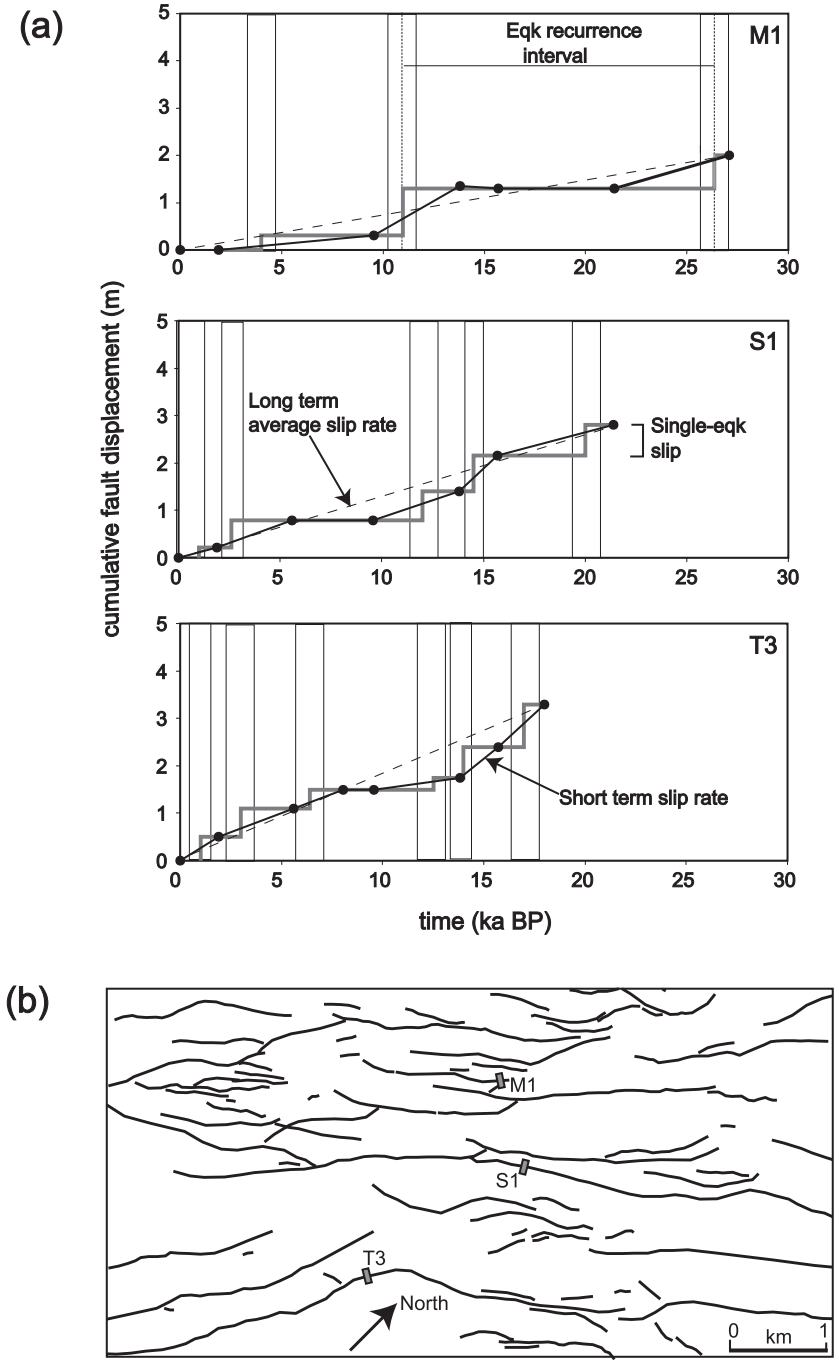

Figure 11. (a) Displacement time plots derived from trenches (M1, S1 and T3) dug along three subparallel normal faults within the Taupo Rift, New Zealand, (b) shows location of trenches and map pattern of fault array (modified from Nicol *et al*. 2010). In (a), filled black circles indicate displacements of dated horizons, although the black line shows the displacement accumulation observed in each trench. The grey stepped line shows slip increments during individual palaeoearthquakes; inferred uncertainties in the timing of palaeoearthquakes are indicated by the grey polygons. Dashed line is long-term average slip rate (SR_{mean}).

is located in the stress shadow of Site 5, that is, across-strike, and vice versa. Both sites are loaded by ruptures occurring along-strike, as they will lie in the stress enhancement zone of these elements. However, depending on the trajectory of propagation through the zone where the fault splits, either Site 4 or 5 will be unloaded. Once the rupture has passed beyond the zone where Sites 4 and 5 are located these elements are again loaded by along-strike stress enhancement so the stress levels recover.

Fig. 12 clearly shows that the stress level and the likelihood of rupture occurring on particular lattice element depend strongly on where each earthquake initiates and the trajectory of propagation, which ultimately depends on the geometry of the fault zone and the orientation of neighbouring ruptures. The magnitude of the stress drop, δ, does influence the spatial extent of the stress variations but does not lead to significant changes in the relationship between SR_{mean}, SRV and CV (insets d and e in Fig. 5; Section 4.1).

© 2012 The Authors, *GJI*
Geophysical Journal International © 2012 RAS

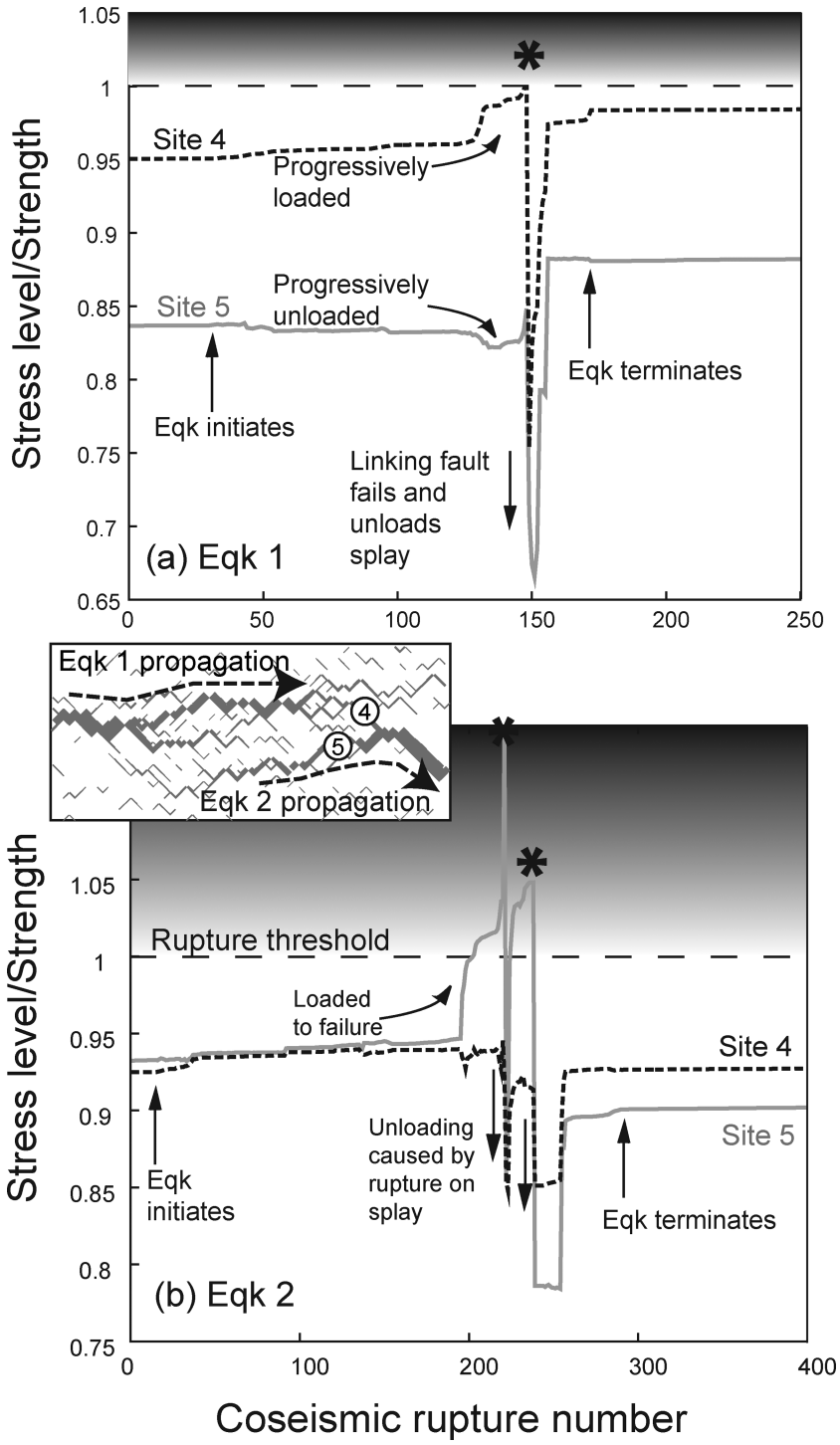

Figure 12. Plots of stress variation during individual earthquakes within the numerical model (a) Earthquake 1 and (b) Earthquake 2, shown to illustrate loading and unloading at Sites 4 and 5 located in Fig. 6(b). The 'coseismic rupture number' is the sequential order of ruptures that comprise one earthquake and is distinct from the 'model time step' measured in years (see Sections 3 and 5.2).

The important role played by fault zone geometry in controlling stress variations spatially, and through time, explains the systematic relationships between CV, SRV and SR_{mean} that we observe in this model (Figs 2–7) as well as the variation in earthquake recurrence distributions (Fig. 8; Tables 1 and 2). For example, it is the combination of stress enhancement and unloading (stress shadowing), occurring sporadically through time (e.g. Fig. 12), which leads to the higher SRV and higher CV in areas where the deformation is partitioned across two faults (Sites 3, 4, 5, 6; Figs 6 and 7). Where this effect is most marked, the distribution of earthquake recurrence intervals becomes exponential and the hazard rate is approximately constant over time (Sites 5 and 6, Fig. 8; Tables 1 and 2). In contrast, the sites with higher average slip rates, lower SRV and CV, quasi-periodic earthquake recurrence and a hazard rate that increases with time (e.g. Sites 1 and 2; Figs 6–8) are located where the dominant effect of other ruptures in the lattice is along-strike stress

© 2012 The Authors, *GJI*
Geophysical Journal International © 2012 RAS

enhancement, which occurs where the fault structure consists of one main strand with a simple geometry.

5.3 Implications for earthquake hazard

Marzocchi *et al*. (2009) modelled coseismic and post-seismic fault interaction within an array of active faults to generate synthetic earthquake catalogues, which they compared to real catalogues of seismicity for the Italian Apennines. One of their key conclusions is that a relatively complex fault pattern is required to generate realistic stochasticity in the seismic catalogue but that this property also prevents a systematic time synchronization of ruptures even on strongly coupled faults. They conclude, therefore, that even though fault interaction is an integral component of the tectonic process, it places strong limits on the forecasting capability of models based on earthquake triggering if stress changes because of the prior history of interaction are not known accurately. In other words, the stress field at a given time in a region is not spatially uniform, as generally assumed in papers seeking to use Coulomb stress transfer calculations to assess the likely locations of future earthquakes, so ruptures often do not occur where predicted. Although our model is simpler than that of Marzocchi *et al*. (2009), our conclusion concerning earthquake forecasting is the same, that is, to assess whether one rupture will trigger further ruptures or not, requires knowledge of current stress levels, which depends primarily on knowledge of prior rupture events rather than the regional tectonic loading (see Section 5.2). Importantly, however, our results are much more encouraging that previous workers suggest because we show that although earthquake activity may appear stochastic on the timescale corresponding to a seismic catalogue, over longer time periods coherent patterns of fault behaviour emerge (Figs 2–8). Therefore, based on this study we recommend that, ideally, information about SRV, and CV derived from palaeoseismology, as well as mapped fault structure and SR_{mean} should be integrated with studies of stress redistribution derived from earthquake records to evaluate seismic hazard.

Our modelling results show that both SRV and CV are required to fully characterize the variability in fault behaviour. Although these parameters both vary with fault geometry and SR_{mean}, SRV contains information about the time ordering of rupture events and the magnitude of the offset, whereas CV does not. Thus, ideally both pieces of information should be used in hazard mapping. Specifically we suggest, based on this modelling study, that:

(1) CV and SRV are higher in areas where the fault pattern is more complex, that is, the deformation is more distributed and SR_{mean} on individual faults is lower. CV and SRV are also likely to be higher where faults intersect and where fault tips are overlapping and extension is being transferred to other fault segments, as shown in Figs 2, 6, 7 and 10.

(2) Significant differences between Quaternary and Holocene slip rates could be interpreted as evidence for higher SRV and CV rather than a changing tectonic regime. These data may be biased towards faults where the slip rate during the Holocene has been higher, as discussed by Nicol *et al*. (2009), but although these faults may be inferred to be the most important in terms of hazard, they may also exhibit long periods of quiescence if they are characterized by higher CV and SRV values. Similarly, faults with subtle Holocene scarps should not be ignored as these may host 'unexpected' events.

(3) Fault with close agreement between rates calculated over different time windows, that is, low SRV, could be used to infer low CV where estimates of CV from palaeoseismology are not available (e.g. compare Sites 1 and 6 in Fig. 7).

(4) Faults that have high average slip rate, low CV and evidence for low SRV, but which also have an elapsed time since the last rupture that is significantly longer than the mean recurrence interval, should ideally be characterized most carefully. Not only could these structures be considered to be close to the end of their 'seismic cycle' (in the sense defined in Section 4.3; Fig. 8), they also impose the strongest long term control on the stress levels of neighbouring faults because they have shorter mean recurrence intervals.

(5) If the Holocene slip rate on a fault is less than the Quaternary rate, and the elapsed time since the last earthquake is long compared to the mean recurrence, this could indicate a fault that is well below its long-term average slip rate. Although this might be consistent with a high SRV, it could indicate that future slip in an earthquake is imminent as such slip is needed to maintain the average slip rate over the longer term.

(6) Incorporating spatial variations in CV and assuming a BPT model of earthquake recurrence does capture some of the variability in recurrence intervals seen in this model, particularly the mean earthquake recurrence and the fall-off in the frequency of longer recurrence intervals. However, it crucially underestimates the number of earthquakes with relatively short recurrence intervals (years to decades for this model, see Fig. 8) which are the hallmark of elastic interaction (Zöller & Hainzl 2007). Ruptures separated by such short recurrence intervals represent significant seismic hazard but may not be recognised as being because of 'stress triggering' as there is unlikely to be clear time synchronization if there is complex fault geometry (e.g. Marzocchi *et al*. 2009). By using a Weibull distribution with fitting parameters that are a function of fault geometry (CV^*, β; Table 2), these effects could be taken into account in hazard studies.

6 CONCLUSIONS

We use a numerical model for elastic interaction between faults, originally presented by Cowie *et al*. (1993), to investigate relationships between fault geometry, fault slip rate variations and the statistics of earthquake recurrence in extensional settings. We analyse the following data extracted from the whole model as well as at specific sites along faults: mean earthquake recurrence, T_{mean}, variability (or aperiodicity) in earthquake recurrence, CV (eq. 1), long-term average slip rate, SR_{mean} (in mm yr^{-1}) and slip rate variability (SRV), obtained by measuring slip rates over a finite time window and comparing it to SR_{mean} (eq. 2). We also extracted histograms of earthquake recurrence and compared these to previously published probability density functions used in earthquake forecasting. Using these data we reach the following conclusions:

(1) SRV is defined for the first time in this paper (eq. 2). Unlike CV, SRV takes into account the time ordering and magnitude of the individual slip events. Its advantage is that it is relatively insensitive to the completeness of the record for smaller magnitude offsets although being highly sensitive to the time order and magnitude of larger magnitude offsets, that is, earthquake clustering. Our modelling results show that both SRV as well as CV are required to fully characterize the variability in fault behaviour.

(2) SRV varies systematically with fault geometry and SR_{mean}. It is larger where the fault system is more complex and SR_{mean} is lower. High values of SRV arise when several earthquakes occur over a relatively short time period (an earthquake cluster) followed by an extended period of relative quiescence. Conversely, where the deformation is localized onto one major fault with a higher SR_{mean}, SRV is low and cumulative displacement history is more

© 2012 The Authors, *GJI*
Geophysical Journal International © 2012 RAS

regular with no obvious earthquake clusters. For the model data analysed here in this study, we find that to first-order SRV is inversely proportional to SR_{mean}.

(3) CV also varies with fault geometry and long-term average slip rate but the correlations are not as pronounced or as systematic as they are for SRV. The reason for this is that CV does not take into account the time ordering and magnitude of the individual slip events and is thus less sensitive to earthquake clustering. In general, the fault segments with low SRV are characterized by $0.7 < CV < 1.0$, with the lowest CV values occurring where the long-term average slip rate is highest. Conversely, the fault segments with higher SRV have $CV > 1.0$, consistent with temporal earthquake clustering.

(4) These observations of SRV and CV derived from the model are consistent with available field observations (e.g. Figs 9–11) although more field data are required to establish the nature of the correlations predicted by this model.

(5) The histograms of earthquake recurrence (Fig. 8) are broadly comparable to various published probability density functions that have been used to describe earthquake recurrence intervals for natural fault systems even though no slip rates are imposed in our model *a priori*. Histogram shape varies systematically along individual faults mirroring the variations in CV described in (3) above. In detail, the BPT model consistently underestimates the number of events with short recurrence intervals (years to decades) at all the sites. In contrast, the Weibull distribution provides a better description of the recurrence histograms, with fitting parameters that vary systematically with position along the fault array (Table 2). At sites where $CV > 1.0$ (SRV is high, SR_{mean} is low), the best-fitting Weibull parameters define an exponential distribution (with a non-zero minimum recurrence interval).

(6) The characteristics listed in 2–5 (above) are correlated with fault geometry via the control that fault structure exerts on earthquake rupture initiation and propagation which in turn influence both spatial and temporal patterns of stress enhancement and stress shadowing. Importantly, these correlations and systematic relationships emerge over time even though on short timescales earthquake activity may appear to be stochastic.

(7) We confirm previous modelling results that show that elastic interaction between faults manifests itself as a higher than expected number of short earthquake recurrence intervals (years to decades) rather than the occurrence of time synchronous events, as is often assumed when stress triggering is considered to be important.

(8) Palaeoseismic data should be collected and analysed with fault zone geometry in mind and information on SRV, CV as well as SR_{mean} should be integrated with data from earthquake catalogues when evaluating seismic hazard.

ACKNOWLEDGMENTS

This work was supported by NERC Standard Grant NE/E01545X/1 and NERC Urgency Grant NE/H003266/1. Andy Nicol generously provided the original graphics shown in Fig. 11 and the associated data analysed in Section 5.1. Diane Doser provided useful comments on an earlier version of this paper. We also acknowledge the helpful comments of two anonymous reviewers.

REFERENCES

Abaimov, S.G., Turcotte, D.L., Shcherbakov, R., Rundle, J.B., Yakovlev, G., Goltz, C. & Newman, W.I., 2008. Earthquakes: recurrence and interoccurrence times, *Pure appl. Geophys.,* **165,** 777–795.

Bouchon, M., 1997. The state of stress on some faults of the San Andreas system as inferred from near-field strong motion data, *J. geophys. Res.,* **102,** 11 731–11 744.

Benedetti, L., Finkel, R., Papanastassiou, D., King, G., Armijo, R., Ryerson, F., Farber, D. & Flerit, F., 2002. Post-glacial slip history of the Sparta fault (Greece) determined by 36Cl cosmogenic dating: evidence for non-periodic earthquakes, *Geophys. Res. Lett.,* **29,** 1246, doi:10.1029/2001GL014510.

Bull, J.M., Barnes, P.M., Lamarche, G., Sanderson, D.J. Cowie, P.A., Taylor S.K. & Dix, J.K., 2006. High-resolution record of displacement accumulation on an active normal fault: implications for models of slip accumulation during repeated earthquakes, *J. Struct. Geol.,* **28,** 1146–1166.

Boncio, P., Pizzi, A., Brozzetti, G., Pomposo, G., Lavecchia, G., Di Naccio, D. & Ferrarini, F., 2010. Coseismic ground deformation of the 6 April 2009 L'Aquila earthquake (central Italy, M_w 6.3), *Geophys. Res. Lett.,* **37,** L06308, doi:10.1029/2010GL042807.

Console, R., Pantosti, D. & D'Addezio, G., 2002. Probabilistic approach to earthquake prediction, *Ann. Geophys.,* **45,** 723–731.

Console, R., Murru, M., Falcone, G. & Catalli, F., 2008. Stress interaction effect on the occurrence probability of characteristic earthquakes in the central Apennines, *J. geophys. Res.,* **113,** doi:10.1-29/2007JB005418.

Cornell, C.A., 1971. Probabilistic analysis of damage to structures under seismic loads, in *Dynamic Waves in Civil Engineering: Proceedings of a Conference Organized by the Society for Earthquake and Civil Engineering Dynamics,* pp. 473–493, eds Howells, D.A., Haigh, I.P. & Taylor, C., John Wiley, New York, NY.

Cowgill, E.R., Gold, D., Chen, X.H., Wang, X.F., Arrowsmith, J.R. & Southon, J., 2009. Low Quaternary slip rate reconciles geodetic and geologic rates along the Altyn Tagh fault, northwestern Tibet, *Geology,* **37,** 647–650.

Cowie, P.A., Vanneste C. & Sornette, D., 1993. Statistical physics model for the spatio-temporal evolution of faults, *J. geophys. Res.,* **98,** 21 809–21 822.

Cowie, P.A., Sornette, D. & Vanneste, C., 1995. Multifractal scaling properties of an organising fault population, *Geophys. J. Int.,* **122,** 457–469.

Cowie, P.A., 1998. A healing-reloading feedback control on the growth rate of seismogenic faults, *J. Struct. Geol.,* **20,** 1075–1087.

Dolan, J.F., Bowman, D.D. & Sammis, C.G., 2007. Long-range and long-term fault interactions in Southern California, *Geology,* **35,** 855–858.

Ellsworth, W.L., Matthews, M.V., Nadeau, R.M., Nishenko, S.P., Reasenberg, P.A. & Simpson, R.W., 1999. A physically-based earthquake recurrence model for estimation of long-term earthquake probabilities, *USGS Open File Rep.,* **522,** 22.

Emergeo Working Group, 2010. Evidence for surface rupture associated with the Mw 6.3 L'Aquila earthquake sequence of April 2009, central Italy, *Terra Nova,* **22,** 43–51, doi:10.1111/j.1365-3121.2009.00915.x.

Falcucci, E. *et al*., 2009. The Paganica fault and surface coseismic ruptures caused by the 6 April 2009 earthquake (L'Aquila, central Italy), *Seism. Res. Lett.,* **80,** 940–950.

Faure Walker, J.P., Roberts, G.P., Sammonds, P.R. & Cowie, P.A., 2010. Comparison of earthquake strains over 10^2 to 10^4 year timescales: insights into variability in the seismic cycle in central Apennines, Italy, *J. geophys. Res.,* **115,** B10418, doi:10.1029/2009JB006462.

Field, E.H. *et al*., 2009. Uniform California earthquake rupture forecast, Version 2 (UCERF 2), *Bull. seism. Soc. Am.,* **99,** 2053–2107, doi:10.1785/0120080049.

Friedrich, A.M., Wernicke, B.P., Niemi, N.A., Bennett, R.A. & Davis, J.L., 2003. Comparison of geodetic and geologic data from the Wasatch region, Utah, and implications for the spectral character of Earth deformation at periods of 10 to 10 million years, *J. geophys. Res.,* **108,** doi:10.1029/2001JB000682.

Galli, P. *et al*., 2009. Il terremotto Aquilano del 6 Aprile 2009: Rilievo macrosismico, effetti di superficie ed implicazioni sismotettoniche, *Il Quaternario,* **22,** 235–246.

King, G.C.P., Stein, R.S. & Lin, J., 1994. Static stress changes and the triggering of earthquakes, *Bull. seism. Soc. Am.,* **84,** 935–953.

© 2012 The Authors, *GJI*
Geophysical Journal International © 2012 RAS

Lyakhovsky, V., Ben Zion, Y. & Agnon, A., 2001. Earthquake cycle, fault zones, and seismicity patterns in a theologically layered lithosphere, *J. geophys. Res.,* **106,** 4103–4120.

Marzocchi, W., Selva, J., Cinti, F.R., Montone, P., Pierdominici, S., Schivardi, R. & Boschi, E., 2009. On the occurrence of large earthquakes: new insights from a model based on interacting faults embedded in a realistic tectonic setting, *J. geophys. Res.,* **114,** doi:10.1029/2008JB006231.

Matthews, M.V., Ellsworth, W.L. & Reasenberg, P.A., 2002. A Brownian model for recurrent earthquakes, *Bull. seism. Soc. Am.,* **92,** 2233–2250.

McClymont, A.F., Villamor, P. & Green, A.G., 2009. Fault displacement accumulation and slip rate variability within the Taupo Rift (New Zealand) based on trench and 3-D ground-penetrating radar data, *Tectonics,* **28,** TC4005, doi:10.1029/2008TC002334.

Mitchell, S.G., Matmon, A., Bierman, P.R., Enzel, Y., Caffee, M. & Rizzo, D., 2001. Displacement history of a limestone normal fault scarp, northern Israel, from cosmogenic ^{36}Cl, *J. geophys. Res.,* **106,** 4247–4264.

Mouslopoulou, V., Walsh, J. & Nicol, A., 2009. Fault displacement rates on a range of timescales, *Earth planet. Sci. Lett.,* **278,** 186–197.

Mucciarelli, M., 2007. A test for checking earthquake aperiodicity estimates from small samples, *Nat. Hazards Earth Syst. Sci.,* **7,** 399–404.

Narteau, C., 2007. Formation and evolution of a population of strike-slip faults in a multiscale cellular automaton model, *Geophys. J. Int.,* **168,** 723–744.

Nicol, A., Walsh, J., Berryman, K. & Villamor, P., 2006. Interdependence of fault displacement rates and paleoearthquakes in an active rift, *Geology,* **34,** 865–868.

Nicol, A., Walsh, J., Mouslopoulou, V. & Villamor, P., 2009. Earthquake histories and Holocene acceleration in fault displacement rates, *Geology,* **37,** 911–914.

Nicol, A., Walsh, J., Villamor, P., Seebeck, H., & Berryman, K.R., 2010. Normal fault interactions, paleoearthquakes and growth in an active rift, *J. Struct. Geol.,* **32,** 1101–1113.

Oskin, M., Perg, L., Shelef, E., Strane, M., Gurney, E., Singer, B. & Zhang, X., 2008. Elevated shear zone loading rate during an earthquake cluster in eastern California, *Geology,* **36,** 507–510.

Pace, B., Peruzza, L., Lavecchia, G. & Boncio, P., 2006. Layered seismogenic source model and probabilistic seismic-hazard analyses in central Italy, *Bull. seism. Soc. Am.,* **96,** 107–132.

Pantosti, D., D'Addezio, G. & Cinti, F.R., 1993. Paleoseismological evidence of repeated large earthquakes along the 1980 Irpinia earthquake fault, *Ann. Geofis.,* **XXXVI**(1), 321–330.

Papanikolaou, I.D., 2003. Generation of high resolution seismic hazard maps in extensional tectonic settings through integration of earthquake geology, fault mechanics theory and GIS techniques. *PhD thesis,* University of London, 437pp.

Papanikolaou, I, Roberts, G.P. & Michetti, A.M., 2005. Fault scarps and deformation rates in Lazio-Abruzzo, central Italy: comparison between geological fault slip-rate and GPS data, *Tectonophysics,* **408,** 147–176.

Parsons, T., 2008. Monte Carlo method for determining earthquake recurrence parameters from short paleoseismic catalogues, example calculations, *J. geophys. Res.,* **113,** B03302, doi:1029/2007JB004998.

Peruzza, L., Pace, B. & Cavallini, F., 2010. Error propagation in time-dependent probability of occurrence for characteristic earthquakes in Italy, *J. Seismol.,* **14,** 119–141.

Pollard, D.D. & Segall, P., 1987. Theoretical displacements and stresses near fractures in rocks: with applications to faults, joints, veins, dikes and solution surfaces, in *Fracture Mechanics of Rock*, pp. 227–350, ed. Atkinson, B.K., Academic Press Inc.,Orlando, FL.

Pizzi, A., Calmita, F., Coltorti, M. & Pieruccini, P., 2002. Quaternary normal faults, intramontane basins and seismicity in the Umbria-Marche Apennines Ridge (Italy): contribution of neotectonic analysis to seismic hazard assessment, *Boll. Soc. Geol. It.,* **1,** 923–929.

Robinson, R., Nicol, A., Walsh, J.J. & Villamor, P., 2009. Features of earthquake recurrence in a complex normal fault network: results from a synthetic seismicity model of the Taupo Rift, New Zealand, *J. geophys. Res.,* **114,** B12306, doi:10.1029/2008JB006231.

Roberts, G.P. & Michetti, A.M., 2004. Spatial and temporal variations in growth rates along active normal fault systems: an example from Lazio-Abruzzo, central Italy, *J. Struct. Geol.,* **26,** 339–376.

Rundle, J.B., Rundle, P.B., Donnellan, A., Li, P., Klein, W., Morein, G., Turcotte, D.L. & Grant, L., 2006. Stress transfer in earthquakes, hazard estimation and ensemble forecasting: inferences from numerical simulations, *Tectonophysics,* **413,** 109–125.

Schlagenhauf, A., Gaudemer, Y., Benedetti, L., Manighetti, I., Palumbo, L., Schimmelpfennig, I., Finkel, R. & Pou, K., 2010. Using in situ Chlorine-36 cosmonuclide to recover past earthquake histories on limestone normal fault scarps: a reappraisal of methodology and interpretations, *Geophys. J. Int.,* **182,** 36–72, doi:10.1111/j.1365-246X.2010.04622.x.

Schlagenhauf, A., Manighetti, I., Benedetti, L., Gaudemer, Y., Finkel, R., Malavieille, J. & Pou, K., 2011. Earthquake supercycles in central Italy inferred from ^{36}Cl exposure dating, *Earth planet. Sci. Letts.,* **307,** 487–500, doi:10.1016/j.epsl.2011.05.022.

Sornette, D., Cowie, P., Miltenberger, P., Sornette A. & Vanneste, C., 1994. Organisation of rupture, *Solid State Phenom.,* **35–36,** 303–318.

Taylor, S.K., Bull, J.M., Lamarche, G. & Barnes, P.M., 2004. Normal fault growth and linkage during the last 1.3 million years: an example from the Whakatane Graben, New Zealand, *J. geophys. Res.,* **109,** B02408, doi:10.1029/2003JB002412.

Zöller, G. & Hainzl, S., 2007. Recurrence time distributions of large earthquakes in a stochastic model for coupled fault systems: the role of fault interaction, *Bull. seism. Soc. Am.,* **97,** 1679–1687.

© 2012 The Authors, *GJI*
Geophysical Journal International © 2012 RAS